Birkbeck
UNIVERSITY OF LONDON

Error Propagation Analysis for a Static Convergent Beam Triple LIDAR

By

T. C. Holtom & A. C. Brooms

Birkbeck Mathematical Sciences Preprint Series Preprint Number 41

www.bbk.ac.uk/ems/research/pure/preprints

Error Propagation Analysis for a Static Convergent Beam Triple LIDAR

Theodore C. Holtom*& Anthony C. Brooms†

August 20, 2019

Abstract

We consider the matter of how to assess uncertainty propagation for the *converging* beam triple LIDAR technology, which is used for measuring wind velocity passing through a fixed point in space. Converging beam triple LIDAR employs the use of three non-parallel, non-coplanar, laser beams which are directed from a fixed platform, typically at ground level, that extend to meet at the point at which measurement of velocity is sought. Coordinate values of the velocity are ascertained with respect to unit vectors along the lines of sight of the laser beams (Doppler vectors), which are then resolved in order to determine the velocity in terms of Cartesian coordinates (i.e. with respect to the standard basis). However, if there is any discrepancy between the recorded values of the coordinates with respect to the Doppler unit vectors and/or the perceived angle settings for such vectors with what they really should be, however small, then this will lead to errors in the reconstructed Cartesian coordinates. One aim of this paper is to present the detailed formulae that would be required for the computation of the estimated variances of the reconstructed velocities, calculated on the basis of the *error propagation formulae* (and to highlight to the practitioner the conditions under which such estimated variances could be relied upon). The other main aim of this paper is to demonstrate that for (various wind profiles and, in particular) certain LIDAR configurations, which can be characterized by an associated parallelepiped with unit edge length, the estimated variances have the potential to be unsuitably large, thus indicating that the reconstructed velocity may be unreliable for gauging the value of the true wind velocity and that the practitioner should avoid such configurations in the measurement campaign.

KEYWORDS: WIND TURBINES; WIND VELOCITY FIELD; CONVERGING BEAM LIDAR; DOPPLER LIDAR; DOPPLER VECTORS; VELOCITY RECONSTRUCTION; MEASUREMENT ERROR; FORWARD ERROR PROPAGATION; ERROR PROPAGATION FORMULA

1 Introduction

Efficient deployment of wind power provides economic benefits, as well as reducing carbon dioxide emissions and other pollution in accordance with UK and international government targets (UK Department of Energy and Climate Change (2013), UK Department of Business, Energy and Industrial Strategy (2018), EU Commission (2017)).

The onshore and offshore wind industry requires wind measurement at the pre-construction site planning stage in order to determine whether a given site has favourable wind conditions and to

*Postal address: Wind Farm Analytics Ltd; 2/1, 3 Queens Park Avenue; Glasgow G42 8BX, U.K. email: info@wind-farm-analytics.co.uk

†Postal address: Birkbeck, University of London; Department of Economics, Mathematics & Statistics; Malet Street; London WC1E 7HX, U.K. email: a.brooms@bbk.ac.uk

estimate the likely energy production from a wind farm located at the given site (MEASNET (2016)). Favourable wind conditions imply firstly that the average wind speed throughout the year is high enough, and secondly that the wind conditions are not too damaging due to excessive gusts, excessive turbulence intensity, extreme non-horizontal flow, or due to other extreme or abnormal flow conditions.

It is noted that site wind conditions vary considerably due to site weather conditions, as well as due to local terrain complexity and terrain roughness features such as forestry. Measurement data may be collected over some years in order to characterise a prospective wind farm site. Statistical and stochastic effects imply that there is uncertainty associated with extrapolating the measured time series data to a future expected wind regime which may be used to predict wind farm output. Reducing measurement uncertainty is beneficial in reducing uncertainty in predicted energy output as well as fatigue loading conditions. Therefore reduced measurement uncertainty allows for reduction in financial uncertainty and enables more efficient deployment of capital and resources.

Also, wind turbines continue to grow in size with rotor diameters as large as 180 metres and top tip height as high as 225 metres. This means that the variation in wind velocity field across the entire rotor area has a significant effect both on energy production, as well as fatigue loading throughout the wind turbine components such as blades, rotating drive train, tower and onshore/offshore foundations. Therefore wind measurement across a large area or volume of space can be beneficial towards optimization of wind farms, both at the pre-construction planning stage, as well as during the operational lifetime of wind farms and their wind turbines.

Traditionally the wind industry has employed mast mounted single point instruments such as spinning cup anemometers, wind vanes and ultrasonic equivalents but in recent years has employed remote sensing methods such as SODAR (SOnic Detection And Ranging) and LIDAR (laser-based Light Detection And Ranging) (Mikkelson pp. 10-23 in Peña et. al. (2015)). A mast may provide a number of measurements at different heights but typically ignores the lateral variation in wind field.

Often the wind flow has been assumed to be horizontal only, or the vertical component neglected, which is not always correct.

LIDAR wind velocity measurement works on the basis of the Doppler effect whereby laser radiation along a given laser line of sight is reflected back along that line of sight from microscopic aerosol particles within the air carried by the wind. The Doppler effect is well known and causes a frequency change in the reflected laser radiation. The frequency change may be measured by suitable signal processing and this provides a measured velocity component along the laser line of sight (see Pitter et. al. pp. 99-130 and Cariou pp. 131-148, in Peña et. al. (2015)).

It is possible to select a measurement range by using timing gates, or "range gates", in the signal processing of pulsed LIDARs – essentially fixing the measurement range by knowledge of the duration of time of flight of radiation there and back, or alternatively by controlling the focus range of focused CW (continuous wave) LIDARs – relying on the fact that the integrated Doppler signal will be dominated by reflected radiation from the optically focused region.

Usually the LIDAR is placed on the ground and, in the typical land-based deployment, the chosen measurement range of interest corresponds to the typical wind turbine hub height, such as 100 metres.

The wind industry has already been employing LIDAR technology. However, the usual deployment of wind LIDAR employs a diverging beam approach. For instance the conical scan approach employs a beam at a fixed angle to a rotation axis and then takes many measurements as the beam rotates around that axis, describing a cone. For instance one hundred measurements might be taken per revolution or conical scan. These measurements along different lines of sight may be combined into a single wind velocity measurement. However, by combining many line of sight measurements in this way there is an implicit assumption of simple wind flow. Effectively the diverging beam LIDAR averages the wind velocity around a circular probe region at a chosen range on the conical scan.

Apart from conical scan, another commonly used diverging beam design is the beam swinging approach where typically four beam directions are employed by switching or swinging the beams. This configuration is equivalent to a conical scan with only four samples around the circle/cone. Both conical scan and beam swinging methods may be referred to as VAD scan (Velocity Azimuth Display). Since it is a special case of conical scan, the beam swinging approach suffers the same problem as the conical scan in that it combines independent line of sight measurements from probe regions which are separated in space, typically by distances of approximately 100 metres.

Therefore the diverging beam LIDAR approach suffers from the assumption of uniform or simple linearly varying flow. The lack of general validity of this assumption gives rise to increased measurement error.

We know from simply observing the motion of leaves and branches of a tree in the wind that the wind is spatially varying and it is wrong to assume uniform or linearly varying flow. Considering that a large wind turbine (of rotor diameter 180 metres) may be ten times greater than the height of a large tree then it is noted that the wind velocity may vary considerably from top to bottom and from left to right across large rotors. Therefore the diverging beam LIDAR approach suffers from measurement ambiguity and measurement error uncertainties arising from the assumption of uniform flow.

In order to properly reconstruct a three dimensional wind velocity vector it is required to measure three independent non-parallel wind components. If the wind velocity vector field is varying non-linearly in space then to measure the wind velocity at a chosen point one should converge three LIDAR beams at the chosen measurement point (Mann et al. 2008). Sathe et al. (2015) (Section 3.2.5) write that "one of the biggest disadvantages of using a single lidar is the necessity of the horizontal homogeneity assumption that almost precludes its use in complex terrains/flows, as well as within wind turbine wakes. We are then forced to use a triple lidar system, where the beams cross at a point".

A single point wind velocity measurement can be obtained by use of three or more fixed converging beam LIDARs. By employing an angle-scanning (or beam switching) LIDAR system with three separate LIDARs scanning (or switching) in cooperation to a succession of measurement points, it is then possible to measure a two-dimensional (planar) or three-dimensional (volumetric) wind velocity field map.

The convergence of three beams accounts for the fact that wind velocity is a three-dimensional vector quantity. The scanning or variation through a succession of measurement points accounts for the fact that the velocity vector field may vary three-dimensionally throughout a volume of space.

Proper measurement of non-horizontal flow, or measurement of yaw error in directional control of operational turbines (Fleming et al. (2014)), are examples of situations where it is beneficial to account for the three-dimensional nature of wind velocity.

Measurement of wind shear (changing wind speed with height, Wagner et al. (2011)) and wind veer (changing wind direction with height) are examples of where it is necessary to measure the three-dimensional variation of wind velocity through space. This may determine suitability of a site for wind turbine deployment.

In summary the measurement of the three-dimensional volumetrically varying wind velocity vector field offers numerous advantages to the wind industry, including that of better site assessment of damaging local conditions, better turbine site classifications (matching turbine strengths to site conditions), and better insurance and warranty conditions (ensuring turbines are operating within their design specifications). This may be achieved by a scanning converging beam triple LIDAR.

Furthermore, converging beam triple LIDAR has potential applications in the aviation and construction industries: these would include, for example, wind limited runway operations, helicopter

operations, crane operations, and bridge operations.

There are two main aims of this paper. One of them is to present, in as a compact and succinct form as possible, suitable for implementation by the practitioner, the detailed formulae that would be required for the computation of the estimated variances of the reconstructed velocities, calculated on the basis of the *error propagation formulae*. The other main aim is to highlight to the practitioner the LIDAR configurations under which such estimated variances could be very large. The mathematics of this paper provides the means by which LIDAR practitioners can avoid such adverse configurations in order to obtain reliable velocity measurements. We will show that such adverse LIDAR configurations can be characterized by the absolute value of the triple scalar product of the unit vectors characterizing the directions of the laser beams, which in turn translates into the volume of an associated parallelepiped with unit edge length. We will corroborate and help illustrate these theoretical deductions with several numerical examples towards the end of the paper.

2 Mathematical Preliminaries and Problem Formulation

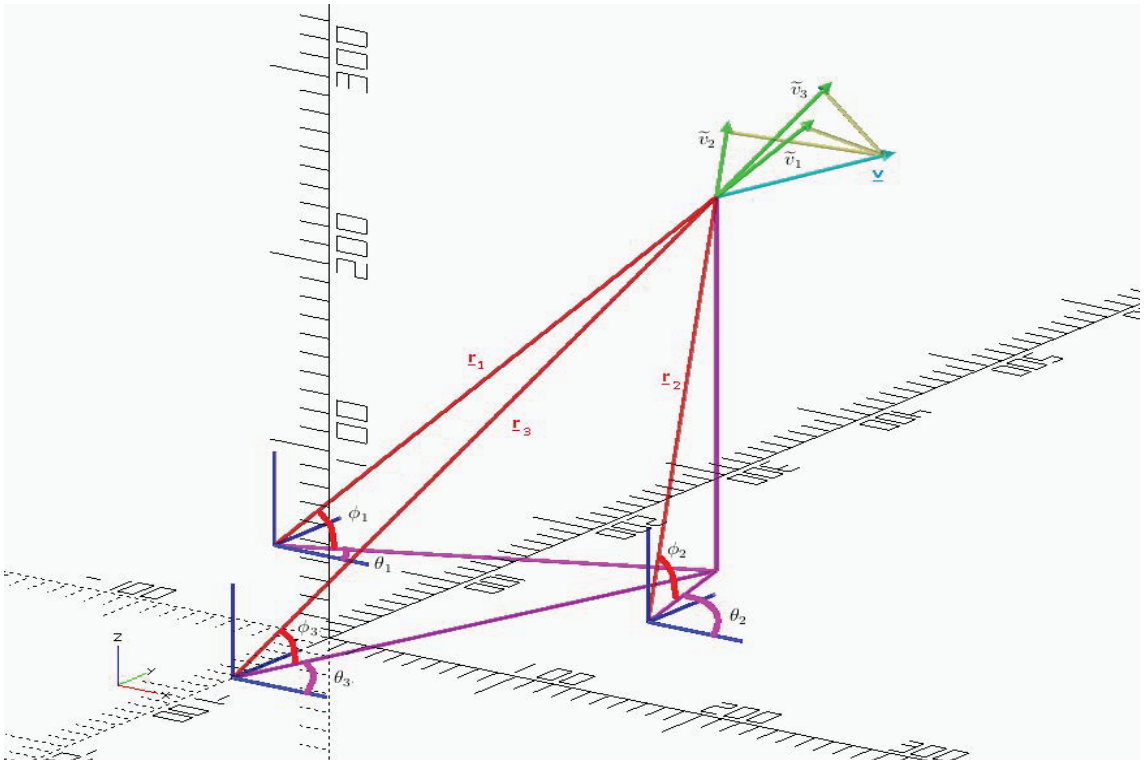

Figure 1: Geometric set-up of the convergent triple-beam LIDAR technology

Throughout we shall work with the index set $\mathcal{I} = \{1, 2, 3\}$. Let $\{\mathbf{e}_i : i \in \mathcal{I}\}$ be the unit vectors for the standard basis in $\mathbb{R}^3$, where $\mathbf{e}_1, \mathbf{e}_2$, and $\mathbf{e}_3$, correspond to the x, y, z directions, respectively, in the right-handed Cartesian coordinate system.

Let $\{\hat{\mathbf{r}}_i : i \in \mathcal{I}\}$ be the unit vectors corresponding to the directions of each of the laser/LIDAR beams i.e. the Doppler LIDAR basis vectors. Thus, from the point of origin of each of the Doppler LIDAR beams, the point in space for which a velocity measurement is being sought, is represented

by $\mathbf{r}_i = \widetilde{r}_i \hat{\mathbf{r}}_i$, for each lidar beam $i \in \mathcal{I}$, respectively.

A wind velocity, $\mathbf{w}$, relative to the aformentioned standard basis may represented as

$$\mathbf{w} = w_1 \mathbf{e}_1 + w_2 \mathbf{e}_2 + w_3 \mathbf{e}_3. \tag{1}$$

Each Doppler LIDAR measurement obtains a component of wind velocity along the LIDAR line of sight. Therefore, employing the scalar product of two vectors (the unit line of sight vector and the wind velocity vector relative to the standard basis) one obtains the Doppler line of sight component, given by

$$\widetilde{w}_i = \hat{\mathbf{r}}_i . \mathbf{w} = \sum_{j \in \mathcal{I}} r_{ij} w_j \ \text{ for all } i \in \mathcal{I}, \tag{2}$$

where $\hat{\mathbf{r}}_i = (r_{i1}, r_{i2}, r_{i3})^T$, for $i \in \mathcal{I}$.

It is to be noted that the unit direction vectors do not depend on the position of the measurement point and in particular the above equation does not depend on the range or distance to the measurement point. Therefore range dependence of the velocity reconstruction exists only in the sense of increasing error on the three Doppler measurements which can be range dependent due to range limitations of LIDAR: however, such considerations will be ignored for the purposes of this discussion.

For each Doppler unit vector $\hat{\mathbf{r}}_i$, $i \in \mathcal{I}$, we may characterize its direction by:
$\theta_i \in [0, 2\pi)$, the azimuthal angle measured anti-clockwise from the x-axis; $\phi_i \in [-\pi/2, \pi/2]$, the elevation angle from the (x, y)-plane, taken to be positive when the z-coordinate is positive (as would normally be the case for a platform set on the ground measuring a point that is above ground). Then each of the Doppler unit vectors can be re-expressed in terms of the standard basis as follows:

$$\hat{\mathbf{r}}_i = \cos(\theta_i)\cos(\phi_i)\mathbf{e}_1 + \sin(\theta_i)\cos(\phi_i)\mathbf{e}_2 + \sin(\phi_i)\mathbf{e}_3 \quad i \in \mathcal{I}. \tag{3}$$

Equations (2) and (3) can also be written in matrix form:

$$\widetilde{\mathbf{w}} = \mathbf{M}\mathbf{w} \tag{4}$$

where

$$\mathbf{M}_{i1} = r_{i1} = \cos(\theta_i)\cos(\phi_i), \ \ i \in \mathcal{I} \tag{5}$$

$$\mathbf{M}_{i2} = r_{i2} = \sin(\theta_i)\cos(\phi_i), \ \ i \in \mathcal{I} \tag{6}$$

$$\mathbf{M}_{i3} = r_{i3} = \sin(\phi_i), \ \ i \in \mathcal{I} \tag{7}$$

and

$$\widetilde{w}_i = \sum_{j \in \mathcal{I}} \mathbf{M}_{ij} w_j = \cos(\theta_i)\cos(\phi_i)w_1 + \sin(\theta_i)\cos(\phi_i)w_2 + \sin(\phi_i)w_3, \quad i \in \mathcal{I}. \tag{8}$$

It will be assumed throughout the remainder of this paper that $\mathbf{M}$ *is of full rank.*

Thus, given the 6 Doppler angles and the 3 Doppler wind velocity coordinates, one can determine the equivalent co-ordinate representation of the wind velocity with respect to the standard basis:

$$\mathbf{w} = \mathbf{M}^{-1}\widetilde{\mathbf{w}} \tag{9}$$

or, equivalently,

$$w_j = \sum_{k \in \mathcal{I}} [\mathbf{M}^{-1}]_{jk} \widetilde{w}_k \quad j \in \mathcal{I}. \tag{10}$$

Therefore, with knowledge of the elements of $\mathbf{M}$, then $\mathbf{M}^{-1}$ can be obtained. Knowledge of $\mathbf{M}^{-1}$ allows us to estimate the true wind velocity (within the Cartesian reference frame) from the three Doppler LIDAR measured velocity components via an appropriate analogue of equation (9).

Epistemic uncertainty (also known as *systematic uncertainty*) is due to things that one could know about, in principle, but yet do not know about, in practice. For example, this could reflect the notion that some quantity could be measured or ascertained exactly but yet has not been, normally due to the existence of a constraint on the amount of resource (in terms of time, money, technology, etc.) that is able to be applied to such an endeavour. The overall uncertainty may be considered to consist of epistemic uncertainty combined with *aleatoric uncertainty* (also known as *statistical uncertainty*, representative of random unknowns that differ each time we run the same experiment).

It will be our objective in the remainder of this paper to gauge the effect of uncertainty (epistemic or otherwise), as a result of the perceived polar angles and measurements of the Doppler velocity components, on the value of the reconstructed velocity vector in Cartesian coordinates. This will be done by working with a metric commonly referred to as the error propagation formula, which is, in part, derived from a first order Taylor expansion of the output variable around some nominal input configurations. This sort of approach, which normally has to be established on a bespoke basis for the system at hand, has at least been alluded to in the work of Liu et al. (2018), Ni et al. (2016), and Wang et al. (2018).

3 Uncertainty quantification of the components of the reconstructed velocity vector via the error propagation formula

3.1 Derivation of the error propagation formulae

It is noted from (5)-(7) that the entries of $\mathbf{M}^{-1}$ do not involve the Doppler LIDAR components, i.e.:

$$[\mathbf{M}^{-1}]_{jk} = [\mathbf{M}^{-1}]_{jk}(\theta_1, \theta_2, \theta_3, \phi_1, \phi_2, \phi_3), \ j, k \in \mathcal{I}. \tag{11}$$

Generically, we set

$$\boldsymbol{\theta} = (\theta_1, \theta_2, \theta_3)^T \quad \boldsymbol{\phi} = (\phi_1, \phi_2, \phi_3)^T$$

for the azimuthal angles and elevation angles, respectively.

Suppose that at a given measurement position, the true (Cartesian) velocity vector is denoted by $\mathbf{v}^{\text{true}}$, where

$$\mathbf{v}^{\text{true}} = (v_1^{\text{true}}, v_2^{\text{true}}, v_3^{\text{true}})$$

and that the true azimuthal angles, and true elevation angles, of the LIDAR beams, are given by

$$\boldsymbol{\theta}^{\text{true}} = (\theta_1^{\text{true}}, \theta_2^{\text{true}}, \theta_3^{\text{true}})$$

and

$$\boldsymbol{\phi}^{\text{true}} = (\phi_1^{\text{true}}, \phi_2^{\text{true}}, \phi_3^{\text{true}})$$

respectively.

The corresponding *Doppler velocity*, which we shall denote as $\widetilde{\mathbf{v}}^c(\mathbf{v}^{\text{true}}; \boldsymbol{\theta}^{\text{true}}, \boldsymbol{\phi}^{\text{true}})$, consistent with the coordinate transformation equation (4), is given by the following:

$$\widetilde{\mathbf{v}}^c(\mathbf{v}^{\text{true}}; \boldsymbol{\theta}^{\text{true}}, \boldsymbol{\phi}^{\text{true}}) := \mathbf{M}(\boldsymbol{\theta}^{\text{true}}, \boldsymbol{\phi}^{\text{true}})\mathbf{v}^{\text{true}}. \tag{12}$$

In practice, there would be no reasonable expectation that the true velocity vector, $\mathbf{v}^{\text{true}}$, would be available for direct observation (not least because, in general, the LIDAR orientations would be different from those corresponding to the standard basis): thus, in effect, $\mathbf{v}^{\text{true}}$ would be hidden from the observer (only to be eventually discerned via some transformation of a measured Doppler velocity). To emphasise the latent nature of $\mathbf{v}^{\text{true}}$, and its interplay with $(\boldsymbol{\theta}, \boldsymbol{\phi})$ (which, in effect, serve as parameters), we will sometimes suppress display of $\mathbf{v}^{\text{true}}$ by replacing it with "$\bullet$" in its stead: thus, for example, $\widetilde{\mathbf{v}}^c(\mathbf{v}^{\text{true}}; \boldsymbol{\theta}^{\text{true}}, \boldsymbol{\phi}^{\text{true}})$ can be written as $\widetilde{\mathbf{v}}^c(\bullet; \boldsymbol{\theta}^{\text{true}}, \boldsymbol{\phi}^{\text{true}})$.

In practice, we will not be able to ascertain $(\boldsymbol{\theta}^{\text{true}}, \boldsymbol{\phi}^{\text{true}})$ nor the corresponding $\widetilde{\mathbf{v}}^c(\bullet; \boldsymbol{\theta}^{\text{true}}, \boldsymbol{\phi}^{\text{true}})$, but rather we attempt to gauge their values on the basis of nominal estimates. To that end, we will work with generic $(\boldsymbol{\theta}, \boldsymbol{\phi}, \widetilde{\mathbf{v}})$. It will be assumed that $(\boldsymbol{\theta}, \boldsymbol{\phi}, \widetilde{\mathbf{v}}) \in \mathcal{D}$ where

$$\mathcal{D} := \Theta \times \Phi \times \widetilde{V}.$$

Typically, each of Θ, Φ and $\widetilde{V}$ (and therefore $\mathcal{D}$) will be convex.

Let $\mathbf{v} = (v_1, v_2, v_3)^T$ denote the *reconstructed velocity vector*, whose j-th element, $j \in \mathcal{I}$, is defined as follows:

$$v_j := \sum_{k \in \mathcal{I}} [\mathbf{M}^{-1}]_{jk} (\boldsymbol{\theta}, \boldsymbol{\phi}) \, \widetilde{v}_k. \tag{13}$$

In the case in which $(\boldsymbol{\theta}, \boldsymbol{\phi})$ takes the value $(\boldsymbol{\theta}^{\text{true}}, \boldsymbol{\phi}^{\text{true}})$, and $\widetilde{\mathbf{v}}$ takes the value $\widetilde{\mathbf{v}}^c(\mathbf{v}^{\text{true}}; \boldsymbol{\theta}^{\text{true}}, \boldsymbol{\phi}^{\text{true}})$, then it follows that $\mathbf{v}$ will take the value $\mathbf{v}^{\text{true}}$. However, in general, $(\boldsymbol{\theta}, \boldsymbol{\phi}, \widetilde{\mathbf{v}})$ will be chosen to be estimates of $(\boldsymbol{\theta}^{\text{true}}, \boldsymbol{\phi}^{\text{true}}, \widetilde{\mathbf{v}}^c(\mathbf{v}^{\text{true}}; \boldsymbol{\theta}^{\text{true}}, \boldsymbol{\phi}^{\text{true}}))$, in which case $\mathbf{v}$ will correspond to an estimate of $\mathbf{v}^{\text{true}}$.

One notes that the reconstructed velocity vector components can be decomposed in terms of six arbitrarily chosen angles governing the LIDAR orientations and the corresponding assigned Doppler LIDAR components, i.e.

$$v_j = v_j(\boldsymbol{\theta}, \boldsymbol{\phi}, \widetilde{\mathbf{v}}). \tag{14}$$

In the context of a particular measurement scenario, let $\boldsymbol{\theta}_0$ and $\boldsymbol{\phi}_0$ represent the demanded azimuthal angles and demanded elevation angles, respectively. Let $\widetilde{\mathbf{v}}_0(\bullet; \boldsymbol{\theta}_0, \boldsymbol{\phi}_0)$ represent the Doppler velocities that were recorded on the premise of the LIDAR orientations being governed exactly by $(\boldsymbol{\theta}_0, \boldsymbol{\phi}_0)$. Denote the measurement errors around $\boldsymbol{\theta}_0$, $\boldsymbol{\phi}_0$, and $\widetilde{\mathbf{v}}_0(\bullet; \boldsymbol{\theta}_0, \boldsymbol{\phi}_0)$ by $\boldsymbol{\delta\theta}(\boldsymbol{\theta}_0, \boldsymbol{\phi}_0, \widetilde{\mathbf{v}}_0(\bullet; \boldsymbol{\theta}_0, \boldsymbol{\phi}_0))$, $\boldsymbol{\delta\phi}(\boldsymbol{\theta}_0, \boldsymbol{\phi}_0, \widetilde{\mathbf{v}}_0(\bullet; \boldsymbol{\theta}_0, \boldsymbol{\phi}_0))$ and $\boldsymbol{\delta\widetilde{v}}(\boldsymbol{\theta}_0, \boldsymbol{\phi}_0, \widetilde{\mathbf{v}}_0(\bullet; \boldsymbol{\theta}_0, \boldsymbol{\phi}_0))$, respectively (of which $(0, 0, 0)^T$ is a possible realization of each); and set

$$\boldsymbol{\delta x}(\boldsymbol{\theta}_0, \boldsymbol{\phi}_0, \widetilde{\mathbf{v}}_0(\bullet; \boldsymbol{\theta}_0, \boldsymbol{\phi}_0))^T$$
$$= \left[\boldsymbol{\delta\theta}(\boldsymbol{\theta}_0, \boldsymbol{\phi}_0, \widetilde{\mathbf{v}}_0(\bullet; \boldsymbol{\theta}_0, \boldsymbol{\phi}_0))^T, \boldsymbol{\delta\phi}(\boldsymbol{\theta}_0, \boldsymbol{\phi}_0, \widetilde{\mathbf{v}}_0(\bullet; \boldsymbol{\theta}_0, \boldsymbol{\phi}_0))^T, \boldsymbol{\delta\widetilde{v}}(\boldsymbol{\theta}_0, \boldsymbol{\phi}_0, \widetilde{\mathbf{v}}_0(\bullet; \boldsymbol{\theta}_0, \boldsymbol{\phi}_0))^T\right].$$

The measurement errors (which, it is assumed, can never be determined exactly or, indeed, directly observed) are, for convenience, modelled as random variables, parameterized by $\boldsymbol{\theta}_0$, $\boldsymbol{\phi}_0$, and $\widetilde{\mathbf{v}}_0(\bullet; \boldsymbol{\theta}_0, \boldsymbol{\phi}_0)$. Thus, for the measurement scenario under consideration, the true azimuthal angles, true elevation angles, and true Doppler velocities, will be modelled by

$$\boldsymbol{\theta}^*(\boldsymbol{\theta}_0, \boldsymbol{\phi}_0, \widetilde{\mathbf{v}}_0(\bullet; \boldsymbol{\theta}_0, \boldsymbol{\phi}_0)) = \boldsymbol{\theta}_0 + \boldsymbol{\delta\theta}(\boldsymbol{\theta}_0, \boldsymbol{\phi}_0, \widetilde{\mathbf{v}}_0(\bullet; \boldsymbol{\theta}_0, \boldsymbol{\phi}_0));$$

$$\boldsymbol{\phi}^*(\boldsymbol{\theta}_0, \boldsymbol{\phi}_0, \widetilde{\mathbf{v}}_0(\bullet; \boldsymbol{\theta}_0, \boldsymbol{\phi}_0)) = \boldsymbol{\phi}_0 + \boldsymbol{\delta\phi}(\boldsymbol{\theta}_0, \boldsymbol{\phi}_0, \widetilde{\mathbf{v}}_0(\bullet; \boldsymbol{\theta}_0, \boldsymbol{\phi}_0));$$

$$\widetilde{\mathbf{v}}^*(\boldsymbol{\theta}_0, \boldsymbol{\phi}_0, \widetilde{\mathbf{v}}_0(\bullet; \boldsymbol{\theta}_0, \boldsymbol{\phi}_0)) = \widetilde{\mathbf{v}}_0(\bullet; \boldsymbol{\theta}_0, \boldsymbol{\phi}_0) + \boldsymbol{\delta\widetilde{v}}(\boldsymbol{\theta}_0, \boldsymbol{\phi}_0, \widetilde{\mathbf{v}}_0(\bullet; \boldsymbol{\theta}_0, \boldsymbol{\phi}_0)).$$

Although $\widetilde{\mathbf{v}}_0(\bullet;\boldsymbol{\theta}_0,\boldsymbol{\phi}_0)$ may be regarded as a realization of a random variable, in terms of the modelling of $\widetilde{\mathbf{v}}^*(\boldsymbol{\theta}_0,\boldsymbol{\phi}_0,\widetilde{\mathbf{v}}_0(\bullet;\boldsymbol{\theta}_0,\boldsymbol{\phi}_0))$, however, the former will be treated as fixed (on account of it being directly observed from the instrumentation) with all remaining stochasticity being accounted for by $\boldsymbol{\delta\widetilde{v}}(\boldsymbol{\theta}_0,\boldsymbol{\phi}_0,\widetilde{\mathbf{v}}_0(\bullet;\boldsymbol{\theta}_0,\boldsymbol{\phi}_0))$.

We now proceed to introduce some assumptions that will be useful in order to progress with our analysis.

Assumption 1 (LIDAR beam convergence within a locale of the measurement position)**.**
Given a triple LIDAR locational layout, the LIDAR beams will be assumed to be converging at the originally intended measurement position, $(\boldsymbol{\theta},\boldsymbol{\phi},\widetilde{r}_1,\widetilde{r}_2,\widetilde{r}_3)$ say, (where there would be angular and distance uncertainty in an actual physical deployment) for some sufficiently small region $\boldsymbol{\epsilon}_{\text{locale}} \subseteq \mathbb{R}^6 \times \mathbb{R}^3$ such that $(\boldsymbol{\theta},\boldsymbol{\phi},\widetilde{r}_1,\widetilde{r}_2,\widetilde{r}_3) \in \boldsymbol{\epsilon}_{\text{locale}}$.

The above assumption is easy to justify (and poses no essential loss of generality) in the sense that it is consistent with the notion that, within a small enough locale, the wind flow (expressed within the Cartesian coordinate frame) would exhibit spatial stationarity.

It is also reasonable to suppose that no subset of the components of $\boldsymbol{\delta x}(\boldsymbol{\theta}_0,\boldsymbol{\phi}_0,\widetilde{\mathbf{v}}_0(\bullet;\boldsymbol{\theta}_0,\boldsymbol{\phi}_0))$ has any statistical influence on any other subset, thus leading to the following assumption:

Assumption 2.
The components of $\boldsymbol{\delta x}(\boldsymbol{\theta}_0,\boldsymbol{\phi}_0,\widetilde{\mathbf{v}}_0(\bullet;\boldsymbol{\theta}_0,\boldsymbol{\phi}_0))$ are statistically independent of each other.

Thus the variance-covariance matrices (see Chatfield & Collins (1980), for e.g., for a review of the relevant multivariate statistical concepts) of $\boldsymbol{\delta\theta}(\boldsymbol{\theta}_0,\boldsymbol{\phi}_0,\widetilde{\mathbf{v}}_0(\bullet;\boldsymbol{\theta}_0,\boldsymbol{\phi}_0))$, $\boldsymbol{\delta\phi}(\boldsymbol{\theta}_0,\boldsymbol{\phi}_0,\widetilde{\mathbf{v}}_0(\bullet;\boldsymbol{\theta}_0,\boldsymbol{\phi}_0))$ and $\boldsymbol{\delta\widetilde{v}}(\boldsymbol{\theta}_0,\boldsymbol{\phi}_0,\widetilde{\mathbf{v}}_0(\bullet;\boldsymbol{\theta}_0,\boldsymbol{\phi}_0))$ are given by

$$\boldsymbol{\Sigma}_{\boldsymbol{\delta\theta}}(\boldsymbol{\theta}_0,\boldsymbol{\phi}_0,\widetilde{\mathbf{v}}_0(\bullet;\boldsymbol{\theta}_0,\boldsymbol{\phi}_0))$$

$$= \begin{bmatrix} \sigma^2_{\theta_1}(\boldsymbol{\theta}_0,\boldsymbol{\phi}_0,\widetilde{\mathbf{v}}_0(\bullet;\boldsymbol{\theta}_0,\boldsymbol{\phi}_0)) & 0 & 0 \\ 0 & \sigma^2_{\theta_2}(\boldsymbol{\theta}_0,\boldsymbol{\phi}_0,\widetilde{\mathbf{v}}_0(\bullet;\boldsymbol{\theta}_0,\boldsymbol{\phi}_0)) & 0 \\ 0 & 0 & \sigma^2_{\theta_3}(\boldsymbol{\theta}_0,\boldsymbol{\phi}_0,\widetilde{\mathbf{v}}_0(\bullet;\boldsymbol{\theta}_0,\boldsymbol{\phi}_0))) \end{bmatrix}$$

$$\boldsymbol{\Sigma}_{\boldsymbol{\delta\phi}}(\boldsymbol{\theta}_0,\boldsymbol{\phi}_0,\widetilde{\mathbf{v}}_0(\bullet;\boldsymbol{\theta}_0,\boldsymbol{\phi}_0))$$

$$= \begin{bmatrix} \sigma^2_{\phi_1}(\boldsymbol{\theta}_0,\boldsymbol{\phi}_0,\widetilde{\mathbf{v}}_0(\bullet;\boldsymbol{\theta}_0,\boldsymbol{\phi}_0)) & 0 & 0 \\ 0 & \sigma^2_{\phi_2}(\boldsymbol{\theta}_0,\boldsymbol{\phi}_0,\widetilde{\mathbf{v}}_0(\bullet;\boldsymbol{\theta}_0,\boldsymbol{\phi}_0)) & 0 \\ 0 & 0 & \sigma^2_{\phi_3}(\boldsymbol{\theta}_0,\boldsymbol{\phi}_0,\widetilde{\mathbf{v}}_0(\bullet;\boldsymbol{\theta}_0,\boldsymbol{\phi}_0))) \end{bmatrix}$$

$$\boldsymbol{\Sigma}_{\boldsymbol{\delta\widetilde{v}}}(\boldsymbol{\theta}_0,\boldsymbol{\phi}_0,\widetilde{\mathbf{v}}_0(\bullet;\boldsymbol{\theta}_0,\boldsymbol{\phi}_0))$$

$$= \begin{bmatrix} \sigma^2_{\widetilde{v}_1}(\boldsymbol{\theta}_0,\boldsymbol{\phi}_0,\widetilde{\mathbf{v}}_0(\bullet;\boldsymbol{\theta}_0,\boldsymbol{\phi}_0)) & 0 & 0 \\ 0 & \sigma^2_{\widetilde{v}_2}(\boldsymbol{\theta}_0,\boldsymbol{\phi}_0,\widetilde{\mathbf{v}}_0(\bullet;\boldsymbol{\theta}_0,\boldsymbol{\phi}_0)) & 0 \\ 0 & 0 & \sigma^2_{\widetilde{v}_3}(\boldsymbol{\theta}_0,\boldsymbol{\phi}_0,\widetilde{\mathbf{v}}_0(\bullet;\boldsymbol{\theta}_0,\boldsymbol{\phi}_0))) \end{bmatrix}$$

respectively, with the diagonal forms arising from the absence of correlation between the variables. It follows that the variance-covariance matrix of $\boldsymbol{\delta x}(\boldsymbol{\theta}_0,\boldsymbol{\phi}_0,\widetilde{\mathbf{v}}_0(\bullet;\boldsymbol{\theta}_0,\boldsymbol{\phi}_0))$, a 9×9 matrix, is given by

$$\boldsymbol{\Sigma}_{\boldsymbol{\delta x}}(\boldsymbol{\theta}_0,\boldsymbol{\phi}_0,\widetilde{\mathbf{v}}_0(\bullet;\boldsymbol{\theta}_0,\boldsymbol{\phi}_0))$$

$$= \begin{bmatrix} \boldsymbol{\Sigma}_{\boldsymbol{\theta}}(\boldsymbol{\theta}_0, \boldsymbol{\phi}_0, \widetilde{\mathbf{v}}_0(\bullet; \boldsymbol{\theta}_0, \boldsymbol{\phi}_0)) & \mathbf{0}_{3\times 3} & \mathbf{0}_{3\times 3} \\ \mathbf{0}_{3\times 3} & \boldsymbol{\Sigma}_{\boldsymbol{\phi}}(\boldsymbol{\theta}_0, \boldsymbol{\phi}_0, \widetilde{\mathbf{v}}_0(\bullet; \boldsymbol{\theta}_0, \boldsymbol{\phi}_0)) & \mathbf{0}_{3\times 3} \\ \mathbf{0}_{3\times 3} & \mathbf{0}_{3\times 3} & \boldsymbol{\Sigma}_{\widetilde{\mathbf{v}}}(\boldsymbol{\theta}_0, \boldsymbol{\phi}_0, \widetilde{\mathbf{v}}_0(\bullet; \boldsymbol{\theta}_0, \boldsymbol{\phi}_0)) \end{bmatrix}.$$

Define the gradient operator, $\nabla_{(\boldsymbol{\theta},\boldsymbol{\phi},\widetilde{\mathbf{v}})}$, as

$$\nabla_{(\boldsymbol{\theta},\boldsymbol{\phi},\widetilde{\mathbf{v}})} = \left(\frac{\partial}{\partial\theta_1}, \frac{\partial}{\partial\theta_2}, \frac{\partial}{\partial\theta_3}, \frac{\partial}{\partial\phi_1}, \frac{\partial}{\partial\phi_2}, \frac{\partial}{\partial\phi_3}, \frac{\partial}{\partial\widetilde{v}_1}, \frac{\partial}{\partial\widetilde{v}_2}, \frac{\partial}{\partial\widetilde{v}_3}\right)^T$$

and the Hessian operator, $\widehat{\mathcal{H}}$, a *symmetric matrix*, as

$$\widehat{\mathcal{H}} = \begin{bmatrix} \frac{\partial^2}{\partial\theta_1^2} & \frac{\partial^2}{\partial\theta_1\partial\theta_2} & \frac{\partial^2}{\partial\theta_1\partial\theta_3} & \frac{\partial^2}{\partial\theta_1\partial\phi_1} & \frac{\partial^2}{\partial\theta_1\partial\phi_2} & \frac{\partial^2}{\partial\theta_1\partial\phi_3} & \frac{\partial^2}{\partial\theta_1\partial\widetilde{v}_1} & \frac{\partial^2}{\partial\theta_1\partial\widetilde{v}_2} & \frac{\partial^2}{\partial\theta_1\partial\widetilde{v}_3} \\ \frac{\partial^2}{\partial\theta_2\partial\theta_1} & \frac{\partial^2}{\partial\theta_2^2} & \frac{\partial^2}{\partial\theta_2\partial\theta_3} & \frac{\partial^2}{\partial\theta_2\partial\phi_1} & \frac{\partial^2}{\partial\theta_2\partial\phi_2} & \frac{\partial^2}{\partial\theta_2\partial\phi_3} & \frac{\partial^2}{\partial\theta_2\partial\widetilde{v}_1} & \frac{\partial^2}{\partial\theta_2\partial\widetilde{v}_2} & \frac{\partial^2}{\partial\theta_2\partial\widetilde{v}_3} \\ \frac{\partial^2}{\partial\theta_3\partial\theta_1} & \frac{\partial^2}{\partial\theta_3\partial\theta_2} & \frac{\partial^2}{\partial\theta_3^2} & \frac{\partial^2}{\partial\theta_3\partial\phi_1} & \frac{\partial^2}{\partial\theta_3\partial\phi_2} & \frac{\partial^2}{\partial\theta_3\partial\phi_3} & \frac{\partial^2}{\partial\theta_3\partial\widetilde{v}_1} & \frac{\partial^2}{\partial\theta_3\partial\widetilde{v}_2} & \frac{\partial^2}{\partial\theta_3\partial\widetilde{v}_3} \\ \frac{\partial^2}{\partial\phi_1\partial\theta_1} & \frac{\partial^2}{\partial\phi_1\partial\theta_2} & \frac{\partial^2}{\partial\phi_1\partial\theta_3} & \frac{\partial^2}{\partial\phi_1^2} & \frac{\partial^2}{\partial\phi_1\partial\phi_2} & \frac{\partial^2}{\partial\phi_1\partial\phi_3} & \frac{\partial^2}{\partial\phi_1\partial\widetilde{v}_1} & \frac{\partial^2}{\partial\phi_1\partial\widetilde{v}_2} & \frac{\partial^2}{\partial\phi_1\partial\widetilde{v}_3} \\ \frac{\partial^2}{\partial\phi_2\partial\theta_1} & \frac{\partial^2}{\partial\phi_2\partial\theta_2} & \frac{\partial^2}{\partial\phi_2\partial\theta_3} & \frac{\partial^2}{\partial\phi_2\partial\phi_1} & \frac{\partial^2}{\partial\phi_2^2} & \frac{\partial^2}{\partial\phi_2\partial\phi_3} & \frac{\partial^2}{\partial\phi_2\partial\widetilde{v}_1} & \frac{\partial^2}{\partial\phi_2\partial\widetilde{v}_2} & \frac{\partial^2}{\partial\phi_2\partial\widetilde{v}_3} \\ \frac{\partial^2}{\partial\phi_3\partial\theta_1} & \frac{\partial^2}{\partial\phi_3\partial\theta_2} & \frac{\partial^2}{\partial\phi_3\partial\theta_3} & \frac{\partial^2}{\partial\phi_3\partial\phi_1} & \frac{\partial^2}{\partial\phi_3\partial\phi_2} & \frac{\partial^2}{\partial\phi_3^2} & \frac{\partial^2}{\partial\phi_3\partial\widetilde{v}_1} & \frac{\partial^2}{\partial\phi_3\partial\widetilde{v}_2} & \frac{\partial^2}{\partial\phi_3\partial\widetilde{v}_3} \\ \frac{\partial^2}{\partial\widetilde{v}_1\partial\theta_1} & \frac{\partial^2}{\partial\widetilde{v}_1\partial\theta_2} & \frac{\partial^2}{\partial\widetilde{v}_1\partial\theta_3} & \frac{\partial^2}{\partial\widetilde{v}_1\partial\phi_1} & \frac{\partial^2}{\partial\widetilde{v}_1\partial\phi_2} & \frac{\partial^2}{\partial\widetilde{v}_1\partial\phi_3} & \frac{\partial^2}{\partial\widetilde{v}_1^2} & \frac{\partial^2}{\partial\widetilde{v}_1\partial\widetilde{v}_2} & \frac{\partial^2}{\partial\widetilde{v}_1\partial\widetilde{v}_3} \\ \frac{\partial^2}{\partial\widetilde{v}_2\partial\theta_1} & \frac{\partial^2}{\partial\widetilde{v}_2\partial\theta_2} & \frac{\partial^2}{\partial\widetilde{v}_2\partial\theta_3} & \frac{\partial^2}{\partial\widetilde{v}_2\partial\phi_1} & \frac{\partial^2}{\partial\widetilde{v}_2\partial\phi_2} & \frac{\partial^2}{\partial\widetilde{v}_2\partial\phi_3} & \frac{\partial^2}{\partial\widetilde{v}_2\partial\widetilde{v}_1} & \frac{\partial^2}{\partial\widetilde{v}_2^2} & \frac{\partial^2}{\partial\widetilde{v}_2\partial\widetilde{v}_3} \\ \frac{\partial^2}{\partial\widetilde{v}_3\partial\theta_1} & \frac{\partial^2}{\partial\widetilde{v}_3\partial\theta_2} & \frac{\partial^2}{\partial\widetilde{v}_3\partial\theta_3} & \frac{\partial^2}{\partial\widetilde{v}_3\partial\phi_1} & \frac{\partial^2}{\partial\widetilde{v}_3\partial\phi_2} & \frac{\partial^2}{\partial\widetilde{v}_3\partial\phi_3} & \frac{\partial^2}{\partial\widetilde{v}_3\partial\widetilde{v}_1} & \frac{\partial^2}{\partial\widetilde{v}_3\partial\widetilde{v}_2} & \frac{\partial^2}{\partial\widetilde{v}_3^2} \end{bmatrix}.$$

Set

$$\mathbf{g}_j(\boldsymbol{\theta}_0, \boldsymbol{\phi}_0, \widetilde{\mathbf{v}}_0(\bullet; \boldsymbol{\theta}_0, \boldsymbol{\phi}_0)) = \nabla_{(\boldsymbol{\theta},\boldsymbol{\phi},\widetilde{\mathbf{v}})} v_j(\boldsymbol{\theta}, \boldsymbol{\phi}, \widetilde{\mathbf{v}})\Big|_{(\boldsymbol{\theta}_0,\boldsymbol{\phi}_0,\widetilde{\mathbf{v}}_0(\bullet;\boldsymbol{\theta}_0,\boldsymbol{\phi}_0))}$$

and

$$\mathcal{H}_j((\boldsymbol{\theta}', \boldsymbol{\phi}', \widetilde{\mathbf{v}}')) = \widehat{\mathcal{H}} v_j(\boldsymbol{\theta}, \boldsymbol{\phi}, \widetilde{\mathbf{v}})\Big|_{(\boldsymbol{\theta}',\boldsymbol{\phi}',\widetilde{\mathbf{v}}')}.$$

Justified by the fact that each of the angles governing the LIDAR orientations can, in principle, be set without regard to any other angle, and that (at least from a classical physics perspective) the LIDAR orientations are not deemed to have any effect on the true (Cartesian) wind velocity (and vice-versa), then one observes that for any two distinct variables ξ_1, ξ_2 such that either $\xi_1, \xi_2 \in \Omega_1$, or else $(\xi_1, \xi_2) \in \Omega_1 \times \Omega_2$, where

$$\Omega_1 := \{\theta_1, \theta_2, \theta_3, \phi_1, \phi_2, \phi_3\}$$
$$\Omega_2 := \{v_1^{\text{true}}, v_2^{\text{true}}, v_3^{\text{true}}\},$$

then

$$\frac{\partial \xi_1}{\partial \xi_2} = 0. \tag{15}$$

It can be shown that v_j is twice continuously differentiable on the whole of $\mathbb{R}^3 \times \mathbb{R}^3 \times \mathbb{R}^3$: this follows from (18)-(20) and Propositions 1-4, that point to the fact that the second partial derivatives of v_j (mixed or otherwise) would be nothing more than finite sums of rational functions of sums of finite products of $\sin(\cdot)/\cos(\cdot)$ functions, provided that one rules out the scenario in which the LIDAR directions become either parallel or coplanar (which is guaranteed by the assumption that $\mathbf{M}$ is of full rank – see later discussions in Section 3.2).

In that case, for $(\boldsymbol{\theta}_0, \boldsymbol{\phi}_0, \widetilde{\mathbf{v}}_0) \in \mathcal{D}$, $(\boldsymbol{\theta}^*, \boldsymbol{\phi}^*, \widetilde{\mathbf{v}}^*) \in \mathcal{D}$, one can invoke the Mean Value Theorem (see Section A.6 of Luenberger (2005) for example) to express $v_j(\boldsymbol{\theta}^*, \boldsymbol{\phi}^*, \widetilde{\mathbf{v}}^*)$, whilst suppressing display of $(\bullet; \boldsymbol{\theta}_0, \boldsymbol{\phi}_0)$ on $\widetilde{\mathbf{v}}_0$ and $(\boldsymbol{\theta}_0, \boldsymbol{\phi}_0, \widetilde{\mathbf{v}}_0(\bullet; \boldsymbol{\theta}_0, \boldsymbol{\phi}_0))$ on $(\boldsymbol{\theta}^*, \boldsymbol{\phi}^*, \widetilde{\mathbf{v}}^*)$ for the sake of notational brevity, as

$$v_j(\boldsymbol{\theta}^*, \boldsymbol{\phi}^*, \widetilde{\mathbf{v}}^*) = v_j(\boldsymbol{\theta}_0, \boldsymbol{\phi}_0, \widetilde{\mathbf{v}}_0) + \mathbf{g}_j^T(\boldsymbol{\theta}_0, \boldsymbol{\phi}_0, \widetilde{\mathbf{v}}_0)\boldsymbol{\delta x}(\boldsymbol{\theta}_0, \boldsymbol{\phi}_0, \widetilde{\mathbf{v}}_0)$$

$$+\frac{1}{2}\boldsymbol{\delta x}(\boldsymbol{\theta}_0, \boldsymbol{\phi}_0, \widetilde{\mathbf{v}}_0)^T \mathcal{H}_j\left(\xi\left((\boldsymbol{\theta}_0, \boldsymbol{\phi}_0, \widetilde{\mathbf{v}}_0), (\boldsymbol{\theta}^*, \boldsymbol{\phi}^*, \widetilde{\mathbf{v}}^*)\right)\right)\boldsymbol{\delta x}(\boldsymbol{\theta}_0, \boldsymbol{\phi}_0, \widetilde{\mathbf{v}}_0)$$

where

$$\xi\left((\boldsymbol{\theta}_0, \boldsymbol{\phi}_0, \widetilde{\mathbf{v}}_0), (\boldsymbol{\theta}^*, \boldsymbol{\phi}^*, \widetilde{\mathbf{v}}^*)\right) = (\gamma\boldsymbol{\theta}_0 + (1-\gamma)\boldsymbol{\theta}^*, \gamma\boldsymbol{\phi}_0 + (1-\gamma)\boldsymbol{\phi}^*, \gamma\widetilde{\mathbf{v}}_0 + (1-\gamma)\widetilde{\mathbf{v}}^*)$$

for some $0 \leq \gamma \leq 1$, provided that $\xi\left((\boldsymbol{\theta}_0, \boldsymbol{\phi}_0, \widetilde{\mathbf{v}}_0), (\boldsymbol{\theta}^*, \boldsymbol{\phi}^*, \widetilde{\mathbf{v}}^*)\right) \in \mathcal{D}$ (which will certainly be the case if $\mathcal{D}$ is convex).

In order to proceed further with the analysis of $\mathrm{var}(v_j(\boldsymbol{\theta}^*, \boldsymbol{\phi}^*, \widetilde{\mathbf{v}}^*))$, we briefly review some standard results that will prove to be useful in our endeavour.

Suppose that:
- *X, Y, U, and V, are 1-dimensional random variables;*
- *$\mathbf{X}$ and $\mathbf{Y}$ are two $p \times 1$ random vectors, for some integer $p \geq 1$;*
- *all necessary expectations of positive powers, and pairwise products of positive powers, of X, Y, U, V, (and the components of) $\mathbf{X}$ and $\mathbf{Y}$, can be properly defined and are finite, in order to ensure that all relevant variances and covariances of X, Y, U, V, (and the components of) $\mathbf{X}$ and $\mathbf{Y}$, can be properly defined and are finite;*
- *$\boldsymbol{\Sigma}_{\mathbf{X}}$ is the symmetric, $p \times p$, variance-covariance matrix of $\mathbf{X}$, i.e. $\mathrm{var}(\mathbf{X}) = \boldsymbol{\Sigma}_{\mathbf{X}}$;*
- *a and b are scalar constants;*
- *$\mathbf{c}$ is a $p \times 1$ vector of constants, for some integer $p \geq 1$.*

Then the following hold true:

Property (I)

$$\mathrm{var}(U + V) = \mathrm{var}(U) + \mathrm{var}(V) + 2\mathrm{cov}(U, V).$$

Property (II)

$$\mathrm{var}(\mathbf{c}^T\mathbf{X}) = \mathbf{c}^T\boldsymbol{\Sigma}_{\mathbf{X}}\mathbf{c}.$$

Property (III)

(i)

$$\mathrm{var}(aX) = a^2\mathrm{var}(X).$$

(ii)

$$\mathrm{cov}(aX, bY) = ab\mathrm{cov}(X, Y).$$

Returning to the main calculation, noting that $v_j(\boldsymbol{\theta}_0, \boldsymbol{\phi}_0, \widetilde{\mathbf{v}}_0)$ is a constant (for a particular setting of the demanded angles, along with the perceived Doppler wind velocity measurements) that makes no contribution to variance, and that the variance-covariance matrix of $\boldsymbol{\delta x}(\boldsymbol{\theta}_0, \boldsymbol{\phi}_0, \widetilde{\mathbf{v}}_0)$ is given by $\boldsymbol{\Sigma}_{\boldsymbol{\delta x}}(\boldsymbol{\theta}_0, \boldsymbol{\phi}_0, \widetilde{\mathbf{v}}_0)$, i.e. that

$$\mathrm{var}(\boldsymbol{\delta x}(\boldsymbol{\theta}_0, \boldsymbol{\phi}_0, \widetilde{\mathbf{v}}_0)) = \boldsymbol{\Sigma}_{\boldsymbol{\delta x}}(\boldsymbol{\theta}_0, \boldsymbol{\phi}_0, \widetilde{\mathbf{v}}_0),$$

then it follows, using Property (I), that

$$\begin{aligned}
&\mathrm{var}(v_j(\boldsymbol{\theta}^*, \boldsymbol{\phi}^*, \widetilde{\mathbf{v}}^*)) \\
&= \mathrm{var}\left(\mathbf{g}_j^T(\boldsymbol{\theta}_0, \boldsymbol{\phi}_0, \widetilde{\mathbf{v}}_0)\boldsymbol{\delta x}(\boldsymbol{\theta}_0, \boldsymbol{\phi}_0, \widetilde{\mathbf{v}}_0) + \frac{1}{2}\boldsymbol{\delta x}(\boldsymbol{\theta}_0, \boldsymbol{\phi}_0, \widetilde{\mathbf{v}}_0)^T\mathcal{H}_j(\xi\left((\boldsymbol{\theta}_0, \boldsymbol{\phi}_0, \widetilde{\mathbf{v}}_0), (\boldsymbol{\theta}^*, \boldsymbol{\phi}^*, \widetilde{\mathbf{v}}^*)\right))\boldsymbol{\delta x}(\boldsymbol{\theta}_0, \boldsymbol{\phi}_0, \widetilde{\mathbf{v}}_0)\right) \\
&= \underbrace{\mathrm{var}\left(\mathbf{g}_j^T(\boldsymbol{\theta}_0, \boldsymbol{\phi}_0, \widetilde{\mathbf{v}}_0)\boldsymbol{\delta x}(\boldsymbol{\theta}_0, \boldsymbol{\phi}_0, \widetilde{\mathbf{v}}_0)\right)}_{\text{term (A)}} + \underbrace{\mathrm{var}\left(\frac{1}{2}\boldsymbol{\delta x}(\boldsymbol{\theta}_0, \boldsymbol{\phi}_0, \widetilde{\mathbf{v}}_0)^T\mathcal{H}_j(\xi\left((\boldsymbol{\theta}_0, \boldsymbol{\phi}_0, \widetilde{\mathbf{v}}_0), (\boldsymbol{\theta}^*, \boldsymbol{\phi}^*, \widetilde{\mathbf{v}}^*)\right))\boldsymbol{\delta x}(\boldsymbol{\theta}_0, \boldsymbol{\phi}_0, \widetilde{\mathbf{v}}_0)\right)}_{\text{term (B)}} \\
&+ \underbrace{2\mathrm{cov}\left(\mathbf{g}_j^T(\boldsymbol{\theta}_0, \boldsymbol{\phi}_0, \widetilde{\mathbf{v}}_0)\boldsymbol{\delta x}(\boldsymbol{\theta}_0, \boldsymbol{\phi}_0, \widetilde{\mathbf{v}}_0), \frac{1}{2}\boldsymbol{\delta x}(\boldsymbol{\theta}_0, \boldsymbol{\phi}_0, \widetilde{\mathbf{v}}_0)^T\mathcal{H}_j(\xi\left((\boldsymbol{\theta}_0, \boldsymbol{\phi}_0, \widetilde{\mathbf{v}}_0), (\boldsymbol{\theta}^*, \boldsymbol{\phi}^*, \widetilde{\mathbf{v}}^*)\right))\boldsymbol{\delta x}(\boldsymbol{\theta}_0, \boldsymbol{\phi}_0, \widetilde{\mathbf{v}}_0)\right)}_{\text{term (C)}}.
\end{aligned}$$

Applying Property (II) to (A), Property (III)(i) to (B), and Property (III)(ii) to (C), whilst also collecting together (B) and (C) to form $\mathrm{Err}((\boldsymbol{\theta}_0, \boldsymbol{\phi}_0, \widetilde{\mathbf{v}}_0), (\boldsymbol{\theta}^*, \boldsymbol{\phi}^*, \widetilde{\mathbf{v}}^*))$, yields

$$\mathbf{g}_j^T(\boldsymbol{\theta}_0, \boldsymbol{\phi}_0, \widetilde{\mathbf{v}}_0)\boldsymbol{\Sigma}_{\boldsymbol{\delta x}}(\boldsymbol{\theta}_0, \boldsymbol{\phi}_0, \widetilde{\mathbf{v}}_0)\mathbf{g}_j(\boldsymbol{\theta}_0, \boldsymbol{\phi}_0, \widetilde{\mathbf{v}}_0) + \mathrm{Err}((\boldsymbol{\theta}_0, \boldsymbol{\phi}_0, \widetilde{\mathbf{v}}_0), (\boldsymbol{\theta}^*, \boldsymbol{\phi}^*, \widetilde{\mathbf{v}}^*))$$

where

$$\begin{aligned}
&\mathrm{Err}((\boldsymbol{\theta}_0, \boldsymbol{\phi}_0, \widetilde{\mathbf{v}}_0), (\boldsymbol{\theta}^*, \boldsymbol{\phi}^*, \widetilde{\mathbf{v}}^*)) = \\
&= \frac{1}{4}\mathrm{var}\left(\boldsymbol{\delta x}(\boldsymbol{\theta}_0, \boldsymbol{\phi}_0, \widetilde{\mathbf{v}}_0)^T\mathcal{H}_j(\xi\left((\boldsymbol{\theta}_0, \boldsymbol{\phi}_0, \widetilde{\mathbf{v}}_0), (\boldsymbol{\theta}^*, \boldsymbol{\phi}^*, \widetilde{\mathbf{v}}^*)\right))\boldsymbol{\delta x}(\boldsymbol{\theta}_0, \boldsymbol{\phi}_0, \widetilde{\mathbf{v}}_0)\right) \\
&+\mathrm{cov}\left(\mathbf{g}_j^T(\boldsymbol{\theta}_0, \boldsymbol{\phi}_0, \widetilde{\mathbf{v}}_0)\boldsymbol{\delta x}(\boldsymbol{\theta}_0, \boldsymbol{\phi}_0, \widetilde{\mathbf{v}}_0), \boldsymbol{\delta x}(\boldsymbol{\theta}_0, \boldsymbol{\phi}_0, \widetilde{\mathbf{v}}_0)^T\mathcal{H}_j(\xi\left((\boldsymbol{\theta}_0, \boldsymbol{\phi}_0, \widetilde{\mathbf{v}}_0), (\boldsymbol{\theta}^*, \boldsymbol{\phi}^*, \widetilde{\mathbf{v}}^*)\right))\boldsymbol{\delta x}(\boldsymbol{\theta}_0, \boldsymbol{\phi}_0, \widetilde{\mathbf{v}}_0)\right).
\end{aligned}$$

Now suppose that each one of the nine components of $\boldsymbol{\delta x}(\boldsymbol{\theta}_0, \boldsymbol{\phi}_0, \widetilde{\mathbf{v}}_0)$ lies within the interval $[-\mathcal{B}, \mathcal{B}]$. One can quantify the speed with which $\mathrm{Err}((\boldsymbol{\theta}_0, \boldsymbol{\phi}_0, \widetilde{\mathbf{v}}_0), (\boldsymbol{\theta}^*, \boldsymbol{\phi}^*, \widetilde{\mathbf{v}}^*))$ goes to zero as one reduces the size of $\mathcal{B}$ towards zero also.

Theorem 1. *For fixed nominal input parameters $\boldsymbol{\theta}_0$, $\boldsymbol{\phi}_0$, and $\widetilde{\mathbf{v}}_0$, suppose that*

$$\boldsymbol{\delta x}(\boldsymbol{\theta}_0, \boldsymbol{\phi}_0, \widetilde{\mathbf{v}}_0) \in \mathcal{X} \subseteq [-\mathcal{B}, \mathcal{B}]^9$$

where $\mathcal{B}$ is a positive real number. Then

$$\mathrm{Err}((\boldsymbol{\theta}_0, \boldsymbol{\phi}_0, \widetilde{\mathbf{v}}_0), (\boldsymbol{\theta}^*, \boldsymbol{\phi}^*, \widetilde{\mathbf{v}}^*)) \sim o(\mathcal{B}^\eta) \text{ as } \mathcal{B} \to 0$$

for all $\{\eta : 0 < \eta < 3\}$.

Proof
It can be shown (see Appendix for further details) that an upper bound on $|\mathrm{Err}((\boldsymbol{\theta}_0, \boldsymbol{\phi}_0, \widetilde{\mathbf{v}}_0), (\boldsymbol{\theta}^*, \boldsymbol{\phi}^*, \widetilde{\mathbf{v}}^*))|$ is given by

$$\frac{81}{2}\mathcal{B}^4(\mathcal{H}_j^{\max}(\boldsymbol{\theta}_0, \boldsymbol{\phi}_0, \widetilde{\mathbf{v}}_0))^2 + 54\mathcal{B}^3||\mathbf{g}_j(\boldsymbol{\theta}_0, \boldsymbol{\phi}_0, \widetilde{\mathbf{v}}_0)||\mathcal{H}_j^{\max}(\boldsymbol{\theta}_0, \boldsymbol{\phi}_0, \widetilde{\mathbf{v}}_0) \tag{16}$$

where the norm used throughout the calculation, $||\cdot||$, corresponds to the 2-norm, and that $\mathcal{H}_j^{\max}(\boldsymbol{\theta}_0, \boldsymbol{\phi}_0, \widetilde{\mathbf{v}}_0)$ is an upper bound on the induced norm of the Hessian matrix that arises in the calculation. The result of the theorem follows immediately as a result of the above bound. □

Thus, for all $\{\eta : 0 < \eta < 3\}$,

$$\mathrm{var}(v_j(\boldsymbol{\theta}^*, \boldsymbol{\phi}^*, \widetilde{\mathbf{v}}^*)) = \mathbf{g}_j^T(\boldsymbol{\theta}_0, \boldsymbol{\phi}_0, \widetilde{\mathbf{v}}_0)\boldsymbol{\Sigma}_{\boldsymbol{\delta x}}(\boldsymbol{\theta}_0, \boldsymbol{\phi}_0, \widetilde{\mathbf{v}}_0)\mathbf{g}_j(\boldsymbol{\theta}_0, \boldsymbol{\phi}_0, \widetilde{\mathbf{v}}_0) + o(\mathcal{B}^\eta)$$

$$= s^2_{v_j}(\boldsymbol{\theta}_0, \boldsymbol{\phi}_0, \widetilde{\mathbf{v}}_0) + o(\mathcal{B}^\eta) \text{ as } \mathcal{B} \to 0,$$

where

$$s^2_{v_j}(\boldsymbol{\theta}_0, \boldsymbol{\phi}_0, \widetilde{\mathbf{v}}_0) = \sum_{n \in \mathcal{I}} \left\{ \left(\frac{\partial v_j}{\partial \theta_n} \right)^2 \sigma^2_{\theta_n} + \left(\frac{\partial v_j}{\partial \phi_n} \right)^2 \sigma^2_{\phi_n} + \left(\frac{\partial v_j}{\partial \widetilde{v}_n} \right)^2 \sigma^2_{\widetilde{v}_n} \right\} \Bigg|_{(\boldsymbol{\theta}_0, \boldsymbol{\phi}_0, \widetilde{\mathbf{v}}_0)}. \tag{17}$$

Here $s^2_{v_j}(\boldsymbol{\theta}_0, \boldsymbol{\phi}_0, \widetilde{\mathbf{v}}_0)$ falls within the generic class of expressions known as the *error propagation formulae* (c.f. Taylor (1997) for example): typically, formulae such as these are derived by truncating the expression for $v_j(\boldsymbol{\theta}^*, \boldsymbol{\phi}^*, \widetilde{\mathbf{v}}^*)$ at first order and finding the variance of just that, without actually taking higher order terms into account, as has been done in our deductions. However, the result of Theorem 1 serves only to present the validity of the error propagation formula in a wider context. On the one hand (and the one that would justify truncation prior to taking the variance, as well as the use of the formula in general), if $\mathcal{B}$ were sufficiently small, then $v_j(\boldsymbol{\theta}^*, \boldsymbol{\phi}^*, \widetilde{\mathbf{v}}^*)$ might be deemed to be sufficiently linear across the perturbation domain $[-\mathcal{B}, \mathcal{B}]$[9] to warrant its representation solely by $v_j(\boldsymbol{\theta}_0, \boldsymbol{\phi}_0, \widetilde{\mathbf{v}}_0) + \mathbf{g}_j^T(\boldsymbol{\theta}_0, \boldsymbol{\phi}_0, \widetilde{\mathbf{v}}_0)\boldsymbol{\delta x}(\boldsymbol{\theta}_0, \boldsymbol{\phi}_0, \widetilde{\mathbf{v}}_0)$ (which we can view as a **local strong linearity assumption**): the more linear the representation of $v_j(\boldsymbol{\theta}^*, \boldsymbol{\phi}^*, \widetilde{\mathbf{v}}^*)$, the smaller the absolute values of the entries within the associated Hessian matrix would be. On the other hand, any decrease made to the value of $\mathcal{B}$ would cause a larger proportionate decrease in the upper bound on the variance truncation error as compared to that associated with the value of the error propagation formula where, for example, the input uncertainties are drawn from the uniform distribution (giving rise to variances that are of order $O(\mathcal{B}^2)$ as $\mathcal{B} \to 0$).

To further illustrate the above sentence, it might be the case, for instance, that $\mathcal{B}$ could be reduced by 10%, from $\mathcal{B}$ down to $0.9\mathcal{B}$, due to more accurate measurement of the Doppler velocities and better angle control. The resultant reduction of $\mathcal{B}^2$ down to $0.81\mathcal{B}^2$ would then cause a 19% reduction in the value obtained from the error propagation formula for each of the reconstructed velocity components, whereas the resultant reduction of $\mathcal{B}^3$ down to $0.729\mathcal{B}^3$ would cause the bound on the truncation error (which, as we have already shown, is no worse than of order $O(\mathcal{B}^3)$ as $\mathcal{B} \to 0$) to reduce by at least 27.1%.

Decreases in the value of $\mathcal{B}$ would of course reduce the actual size of the norm of the associated Hessian matrix: but having the linearity assumption to fall back on when $\mathcal{B}$ is at, or below, some critical value, will ensure that $\mathcal{B}$ does not have to be made vanishingly small beyond the level of precision that is capable of being obtained by the instrumentation.

The above arguments suggest that one should regard $s^2_{v_j}(\boldsymbol{\theta}_0, \boldsymbol{\phi}_0, \widetilde{\mathbf{v}}_0)$ as an *estimate* of the variance of $v_j(\boldsymbol{\theta}^*, \boldsymbol{\phi}^*, \widetilde{\mathbf{v}}^*)$ (according to its associated error propagation formula). **The calculation of $s^2_{v_j}(\boldsymbol{\theta}_0, \boldsymbol{\phi}_0, \widetilde{\mathbf{v}}_0)$ will be the focus of our discussion for the remainder of this subsection, and the whole of the next one**.

Along with the values of the variances of the six angles and those of the three measured Doppler velocity components, it is also required to evaluate the partial derivatives that appear in (17).

$$\frac{\partial v_j}{\partial \theta_s} = \sum_{k \in \mathcal{I}} \frac{\partial \left\{ [\mathbf{M}^{-1}]_{jk} \widetilde{v}_k \right\}}{\partial \theta_s} = \sum_{k \in \mathcal{I}} \widetilde{v}_k \frac{\partial [\mathbf{M}^{-1}]_{jk}}{\partial \theta_s} \tag{18}$$

$$\frac{\partial v_j}{\partial \phi_s} = \sum_{k \in \mathcal{I}} \frac{\partial \left\{ [\mathbf{M}^{-1}]_{jk} \widetilde{v}_k \right\}}{\partial \phi_s} = \sum_{k \in \mathcal{I}} \widetilde{v}_k \frac{\partial [\mathbf{M}^{-1}]_{jk}}{\partial \phi_s} \tag{19}$$

$$\frac{\partial v_j}{\partial \widetilde{v}_s} = \sum_{k\in\mathcal{I}} [\mathbf{M}^{-1}]_{jk} \frac{\partial \widetilde{v}_k}{\partial \widetilde{v}_s} = \sum_{k\in\mathcal{I}} [\mathbf{M}^{-1}]_{jk} \delta_{sk} = [\mathbf{M}^{-1}]_{js} \tag{20}$$

where for $l, n \in \mathcal{I}$, δ_{ln} is Kronecker delta.

Thus it will be required to calculate the 27 terms given by $\frac{\partial [\mathbf{M}^{-1}]_{jk}}{\partial \theta_i}$, i,j,$k \in \mathcal{I}$ and the 27 terms $\frac{\partial [\mathbf{M}^{-1}]_{jk}}{\partial \phi_i}$, i,j,$k \in \mathcal{I}$, which in turn will necessitate the calculation of the 6 terms that arise from differentiating Δ, with respect to each of the angles $\theta_1, \theta_2, \theta_3, \phi_1, \phi_2$ and ϕ_3. These matters will be addressed in the next section.

3.2 Computational results pertaining to $\mathbf{M}^{-1}$

The determinant of the matrix $\mathbf{M}$ is given by $\Delta = \Delta(\theta_1, \theta_2, \theta_3, \phi_1, \phi_2, \phi_3)$, a function of the six angles defining three LIDAR beam directions:

$$\begin{aligned}
\Delta = &\cos(\theta_1)\cos(\phi_1)\left\{\sin(\theta_2)\cos(\phi_2)\sin(\phi_3) - \sin(\phi_2)\sin(\theta_3)\cos(\phi_3)\right\} \\
&- \sin(\theta_1)\cos(\phi_1)\left\{\sin(\phi_3)\cos(\theta_2)\cos(\phi_2) - \sin(\phi_2)\cos(\theta_3)\cos(\phi_3)\right\} \\
&+ \sin(\phi_1)\left\{\cos(\theta_2)\cos(\phi_2)\sin(\theta_3)\cos(\phi_3) - \sin(\theta_2)\cos(\phi_2)\cos(\theta_3)\cos(\phi_3)\right\}.
\end{aligned} \tag{21}$$

More compactly, this can be written as

$$\Delta = \sum_{\pi\in S_3} \Delta_\pi \tag{22}$$

where

$$\Delta_\pi := \mathrm{sgn}(\pi)\cos\left(\theta_{\pi(1)}\right)\sin\left(\theta_{\pi(2)}\right)\cos\left(\phi_{\pi(1)}\right)\cos\left(\phi_{\pi(2)}\right)\sin\left(\phi_{\pi(3)}\right) \tag{23}$$

and S_3 is the set of all permutations on $\mathcal{I}$.

In the following lemmas, we will work with the following quantities for identifying particular indices within $\mathcal{I}$ for specific situations.

Definition 1. *For any $l \in \mathcal{I}$, define:*
(i) $K(l) := \mathcal{I}\setminus\{l\}$; *(ii)* $\alpha(l) := \min K(l)$; *(iii)* $\beta(l) := \max K(l)$.

Proposition 1.

$$[\mathbf{M}^{-1}]_{ij} = (-1)^{i+j}\left\{r_{\alpha(j)\alpha(i)}r_{\beta(j)\beta(i)} - r_{\beta(j)\alpha(i)}r_{\alpha(j)\beta(i)}\right\}/\Delta \tag{24}$$

where, for $i' \in \{\alpha(j), \beta(j)\}$ and $j' \in \{\alpha(i), \beta(i)\}$,

$$r_{i'j'} = \begin{cases} \cos(\phi_{i'})\cos(\theta_{i'}) & \text{if } j' = 1 \\ \cos(\phi_{i'})\sin(\theta_{i'}) & \text{if } j' = 2 \\ \sin(\phi_{i'}) & \text{if } j' = 3. \end{cases} \tag{25}$$

Proof
Noting that

$$\mathbf{M} = \begin{bmatrix} r_{11} & r_{12} & r_{13} \\ r_{21} & r_{22} & r_{23} \\ r_{31} & r_{32} & r_{33} \end{bmatrix}$$

then the minor corresponding to the (j,i)-th element of $\mathbf{M}$ is given by

$$r_{\alpha(j)\alpha(i)}r_{\beta(j)\beta(i)} - r_{\beta(j)\alpha(i)}r_{\alpha(j)\beta(i)}.$$

Multiplying this by $(-1)^{i+j}$ gives both the corresponding cofactor of the (j,i)-th element of $\mathbf{M}$ and the (i,j)-th element of the adjoint of $\mathbf{M}$, which, upon dividing through by Δ, yields (24).
Further noting that

$$\mathbf{M} = \begin{bmatrix} \cos(\phi_1)\cos(\theta_1) & \cos(\phi_1)\sin(\theta_1) & \sin(\phi_1) \\ \cos(\phi_2)\cos(\theta_2) & \cos(\phi_2)\sin(\theta_2) & \sin(\phi_2) \\ \cos(\phi_3)\cos(\theta_3) & \cos(\phi_3)\sin(\theta_3) & \sin(\phi_3) \end{bmatrix}$$

then (25) follows. □

Proposition 2. *For $i' \in \{\alpha(j), \beta(j)\}$, $j' \in \{\alpha(i), \beta(i)\}$ and $n \in \mathcal{I}$:*

$$\frac{\partial r_{i'j'}}{\partial \theta_n} = \begin{cases} -\cos(\phi_n)\sin(\theta_n) & \text{if } j' = 1 \text{ and } i' = n \\ \cos(\phi_n)\cos(\theta_n) & \text{if } j' = 2 \text{ and } i' = n \\ 0 & \text{if } j' = 3 \text{ or } i' \neq n \end{cases} \tag{26}$$

and

$$\frac{\partial r_{i'j'}}{\partial \phi_n} = \begin{cases} -\sin(\phi_n)\cos(\theta_n) & \text{if } j' = 1 \text{ and } i' = n \\ -\sin(\phi_n)\sin(\theta_n) & \text{if } j' = 2 \text{ and } i' = n \\ \cos(\phi_n) & \text{if } j' = 3 \text{ and } i' = n \\ 0 & i' \neq n. \end{cases} \tag{27}$$

Proof Follows immediately by differentiating (25) with respect to the $\{\theta_n\}$ and $\{\phi_n\}$. □

Proposition 3.
(i) for each $n \in \mathcal{I}$,

$$\frac{\partial \Delta}{\partial \theta_n} = \sum_{\pi \in S_3} \frac{\partial \Delta_\pi}{\partial \theta_n}$$

where

$$\frac{\partial \Delta_\pi}{\partial \theta_n} = \begin{cases} -\text{sgn}(\pi)\sin\left(\theta_{\pi(1)}\right)\sin\left(\theta_{\pi(2)}\right)\cos\left(\phi_{\pi(1)}\right)\cos\left(\phi_{\pi(2)}\right)\sin\left(\phi_{\pi(3)}\right) & n = \pi(1) \\ \text{sgn}(\pi)\cos\left(\theta_{\pi(1)}\right)\cos\left(\theta_{\pi(2)}\right)\cos\left(\phi_{\pi(1)}\right)\cos\left(\phi_{\pi(2)}\right)\sin\left(\phi_{\pi(3)}\right) & n = \pi(2) \\ 0 & n = \pi(3) \end{cases}$$

(ii) for each $n \in \mathcal{I}$,

$$\frac{\partial \Delta}{\partial \phi_n} = \sum_{\pi \in S_3} \frac{\partial \Delta_\pi}{\partial \phi_n}$$

where

$$\frac{\partial \Delta_\pi}{\partial \phi_n} = \begin{cases} -\text{sgn}(\pi)\cos\left(\theta_{\pi(1)}\right)\sin\left(\theta_{\pi(2)}\right)\sin\left(\phi_{\pi(1)}\right)\cos\left(\phi_{\pi(2)}\right)\sin\left(\phi_{\pi(3)}\right) & n = \pi(1) \\ -\text{sgn}(\pi)\cos\left(\theta_{\pi(1)}\right)\sin\left(\theta_{\pi(2)}\right)\cos\left(\phi_{\pi(1)}\right)\sin\left(\phi_{\pi(2)}\right)\sin\left(\phi_{\pi(3)}\right) & n = \pi(2) \\ \text{sgn}(\pi)\cos\left(\theta_{\pi(1)}\right)\sin\left(\theta_{\pi(2)}\right)\cos\left(\phi_{\pi(1)}\right)\cos\left(\phi_{\pi(2)}\right)\cos\left(\phi_{\pi(3)}\right) & n = \pi(3). \end{cases}$$

Proof
Follows immediately by differentiating (22). □

Proposition 4. *Suppose $\xi_n \in \{\theta_n, \phi_n\}$. Then:*

$$\begin{aligned} \frac{\partial}{\partial \xi_n}[\mathbf{M}^{-1}]_{ij} = \frac{(-1)^{i+j}}{\Delta} \Bigg\{ & r_{\alpha(j)\alpha(i)} \left(\frac{\partial}{\partial \xi_n} r_{\beta(j)\beta(i)} \right) + \left(\frac{\partial}{\partial \xi_n} r_{\alpha(j)\alpha(i)} \right) r_{\beta(j)\beta(i)} \\ & - \left(\frac{\partial}{\partial \xi_n} r_{\beta(j)\alpha(i)} \right) r_{\alpha(j)\beta(i)} - r_{\beta(j)\alpha(i)} \left(\frac{\partial}{\partial \xi_n} r_{\alpha(j)\beta(i)} \right) \Bigg\} \\ & - \frac{(-1)^{i+j}}{\Delta^2} \left\{ r_{\alpha(j)\alpha(i)} r_{\beta(j)\beta(i)} - r_{\beta(j)\alpha(i)} r_{\alpha(j)\beta(i)} \right\} \frac{\partial \Delta}{\partial \xi_n}. \end{aligned} \tag{28}$$

Proof
Follows immediately by differentiating (24). □

3.3 Geometric Interpretation of $|\Delta|$ and its effect on the variance of the reconstructed velocity components

It is noted that the absolute value of the determinant has a geometric interpretation in that it represents the volume of a parallelepiped whose edges are defined by the three unit vectors along the three LIDAR beam directions $\hat{\mathbf{r}}_1$, $\hat{\mathbf{r}}_2$ and $\hat{\mathbf{r}}_3$. Note that the parallelepiped volume is exactly the absolute value of the triple scalar product of $\hat{\mathbf{r}}_1$, $\hat{\mathbf{r}}_2$ and $\hat{\mathbf{r}}_3$. If any two or more of these unit vectors approach each other, or if all three of these vectors approach being co-planar, then the parallelepiped volume tends to zero. On the other hand, the volume is at its maximum when the Doppler vectors are orthogonal to each other, resulting in a parallelepiped that is just a cube of unit length.

It is also to be noted that $|\Delta|$ has the potential to vastly inflate the estimated variances (calculated according to the error propagation formulae (17)) of the reconstructed velocity components: therefore it is recommended to always apply (17), by way of a reliability check of the efficacy of the reconstructed velocities as estimates of the corresponding true velocities, prior to any field deployment, especially when potentially adverse LIDAR configurations have been flagged up, as per the following theorem.

Theorem 2.
Let $\mathcal{C}$ be some closed, feasible, subset of $[0,2\pi)^3 \times [-\frac{\pi}{2},\frac{\pi}{2}]^3 \times \mathbb{R}^3$ for the input parameters and suppose that, for all $n \in \mathcal{I}$, $|\delta\widetilde{v}_n| \leq \mathcal{B} < \infty$.
For a given $j \in \mathcal{I}$, and each $\left(\boldsymbol{\theta}', \boldsymbol{\phi}', \widetilde{\mathbf{v}}'\right) \in \mathcal{C}$ and $n \in \mathcal{I}$, define

$$\widehat{D}_{jn}\left(\boldsymbol{\theta}', \boldsymbol{\phi}', \widetilde{\mathbf{v}}'\right)$$

to be equal to

$$\left|r_{\alpha(n)\alpha(j)}(\boldsymbol{\theta}', \boldsymbol{\phi}')r_{\beta(n)\beta(j)}(\boldsymbol{\theta}', \boldsymbol{\phi}') - r_{\beta(n)\alpha(j)}(\boldsymbol{\theta}', \boldsymbol{\phi}')r_{\alpha(n)\beta(j)}(\boldsymbol{\theta}', \boldsymbol{\phi}')\right| \sqrt{\sigma^2_{\widetilde{v}_j}(\boldsymbol{\theta}', \boldsymbol{\phi}', \widetilde{\mathbf{v}}')}$$

and

$$\underline{D}_{jn}(\mathcal{C}) := \min_{(\boldsymbol{\theta}', \boldsymbol{\phi}', \widetilde{\mathbf{v}}') \in \mathcal{C}} \widehat{D}_{jn}\left(\boldsymbol{\theta}', \boldsymbol{\phi}', \widetilde{\mathbf{v}}'\right).$$

Suppose there exists an $n' \in \mathcal{I}$ such that $\underline{D}_{jn'}(\mathcal{C}) > 0$.

Then for $(\boldsymbol{\theta}_0, \boldsymbol{\phi}_0, \widetilde{\mathbf{v}}_0) \in \mathcal{C}$,
(i)

$$s^2_{v_j}(\boldsymbol{\theta}_0, \boldsymbol{\phi}_0, \widetilde{\mathbf{v}}_0) \geq \frac{\underline{D}^2_{jn'}(\mathcal{C})}{|\Delta(\boldsymbol{\theta}_0, \boldsymbol{\phi}_0)|^2};$$

(ii) $s^2_{v_j}(\boldsymbol{\theta}_0, \boldsymbol{\phi}_0, \widetilde{\mathbf{v}}_0) \to \infty$ as $|\Delta(\boldsymbol{\theta}_0, \boldsymbol{\phi}_0)| \to 0$.

Proof
Using (20), we can deduce that

$$\left(\frac{\partial v_j(\boldsymbol{\theta}', \boldsymbol{\phi}', \widetilde{\mathbf{v}}')}{\partial \widetilde{v}'_n}\right)^2 \sigma^2_{\widetilde{v}_n}(\boldsymbol{\theta}', \boldsymbol{\phi}', \widetilde{\mathbf{v}}') = \left([\mathbf{M}^{-1}]_{jn}(\boldsymbol{\theta}', \boldsymbol{\phi}')\right)^2 \sigma^2_{\widetilde{v}_n}(\boldsymbol{\theta}', \boldsymbol{\phi}', \widetilde{\mathbf{v}}')$$

$$= \left\{\left|[\mathbf{M}^{-1}]_{jn}(\boldsymbol{\theta}', \boldsymbol{\phi}')\right| \sqrt{\sigma^2_{\widetilde{v}_n}(\boldsymbol{\theta}', \boldsymbol{\phi}', \widetilde{\mathbf{v}}')}\right\}^2$$

which, by Proposition 1, is equal to

$$\frac{\left\{ \left| r_{\alpha(n)\alpha(j)}(\boldsymbol{\theta}', \boldsymbol{\phi}') r_{\beta(n)\beta(j)}(\boldsymbol{\theta}', \boldsymbol{\phi}') - r_{\beta(n)\alpha(j)}(\boldsymbol{\theta}', \boldsymbol{\phi}') r_{\alpha(n)\beta(j)}(\boldsymbol{\theta}', \boldsymbol{\phi}') \right| \sqrt{\sigma^2_{\widetilde{v}_j}(\boldsymbol{\theta}', \boldsymbol{\phi}', \widetilde{\mathbf{v}}')} \right\}^2}{|\Delta(\boldsymbol{\theta}', \boldsymbol{\phi}')|^2}$$

and which, by the definition of $\widehat{D}_{jn}(\boldsymbol{\theta}', \boldsymbol{\phi}', \widetilde{\mathbf{v}}')$, equates to

$$\frac{\widehat{D}^2_{jn}(\boldsymbol{\theta}', \boldsymbol{\phi}', \widetilde{\mathbf{v}}')}{|\Delta(\boldsymbol{\theta}', \boldsymbol{\phi}')|^2}.$$

It follows that

$$\sum_{n \in \mathcal{I}} \left\{ \left(\frac{\partial v_j}{\partial \theta_n} \right)^2 \sigma^2_{\theta_n} + \left(\frac{\partial v_j}{\partial \phi_n} \right)^2 \sigma^2_{\phi_n} + \left(\frac{\partial v_j}{\partial \widetilde{v}_n} \right)^2 \sigma^2_{\widetilde{v}_n} \right\} \Bigg|_{(\boldsymbol{\theta}_0, \boldsymbol{\phi}_0, \widetilde{\mathbf{v}}_0)}$$

$$\geq \sum_{n \in \mathcal{I}} \left\{ \left(\frac{\partial v_j}{\partial \widetilde{v}_n} \right)^2 \sigma^2_{\widetilde{v}_n} \right\} \Bigg|_{(\boldsymbol{\theta}_0, \boldsymbol{\phi}_0, \widetilde{\mathbf{v}}_0)} = \sum_{n \in \mathcal{I}} \frac{\widehat{D}^2_{jn}(\boldsymbol{\theta}_0, \boldsymbol{\phi}_0, \widetilde{\mathbf{v}}_0)}{|\Delta(\boldsymbol{\theta}_0, \boldsymbol{\phi}_0)|^2} \geq \frac{\widehat{D}^2_{jn'}(\boldsymbol{\theta}_0, \boldsymbol{\phi}_0, \widetilde{\mathbf{v}}_0)}{|\Delta(\boldsymbol{\theta}_0, \boldsymbol{\phi}_0)|^2} \geq \frac{D^2_{jn'}(\mathcal{C})}{|\Delta(\boldsymbol{\theta}_0, \boldsymbol{\phi}_0)|^2}$$

where the first inequality follows from the non-negativity of the squared terms and of the input parameter variances, the second inequality follows from the non-negativity of the summands, and the final inequality follows from the definition of $\underline{D}_{jn'}(\mathcal{C})$, as required to establish (i).
Part (ii) is a simple corollary of (i). □

Remark: By virtue of the fact that

$$f(\boldsymbol{\theta}', \boldsymbol{\phi}') := \left| r_{\alpha(n)\alpha(j)}(\boldsymbol{\theta}', \boldsymbol{\phi}') r_{\beta(n)\beta(j)}(\boldsymbol{\theta}', \boldsymbol{\phi}') - r_{\beta(n)\alpha(j)}(\boldsymbol{\theta}', \boldsymbol{\phi}') r_{\alpha(n)\beta(j)}(\boldsymbol{\theta}', \boldsymbol{\phi}') \right|$$

is just a composition of a continuous function (namely $|\cdot|$), with another continuous function comprising a linear combination of finite products of $\sin(\cdot)$ and/or $\cos(\cdot)$ functions, then $f(\boldsymbol{\theta}', \boldsymbol{\phi}')$ will itself be continuous with respect to $(\boldsymbol{\theta}', \boldsymbol{\phi}')$, thus ensuring that its minimum (and indeed maximum) over $\mathcal{C}$ exists. Due to the boundedness assumption on the $\{\delta\widetilde{v}_n\}$, one can ensure that the minimum (and indeed a maximum) of $\sigma^2_{\widetilde{v}_n}(\boldsymbol{\theta}', \boldsymbol{\phi}', \widetilde{\mathbf{v}}')$ over $\mathcal{C}$ also exists. Thus, by Cauchy-Schwarz, $\widehat{D}_{jn}(\boldsymbol{\theta}', \boldsymbol{\phi}', \widetilde{\mathbf{v}}')$ is bounded over $\mathcal{C}$ and thus $\underline{D}_{jn}(\mathcal{C})$ is well defined and finite.

4 Numerical Examples

In the following examples, speeds are expressed in metres per second, and angles in radians.

Examples Set 1: varying the demanded elevation angle(s) only
In the scenarios described in this examples set, it will be assumed that the demanded azimuthal angles will be held fixed throughout, but that the elevation angles will change in order to gauge their effect on the results. The value used for the measured Doppler velocity vector will be given by $\widetilde{\mathbf{v}}_0 = \mathbf{M}(\boldsymbol{\theta}_0, \boldsymbol{\phi}_0)\mathbf{v}_0$ for some given Cartesian velocity vector $\mathbf{v}_0$, where $\mathbf{v}_0$ will also be held fixed throughout this examples set. (This will, of course, imply that the same $\mathbf{v}_0$ is being ascertained at different positions in space if the LIDARs are to remain situated at fixed locations; or, otherwise, that $\mathbf{v}_0$ is measured at the same position in space but with the LIDARs moving their locations in order to achieve the required angle orientations).

It will be assumed throughout that the uncertainty ranges around each Doppler velocity, demanded azimuthal angle and demanded elevation angle, will be ± 0.05, ± 0.001, and ± 0.001, respectively. On each of the uncertainty ranges, the true value of the corresponding variable will be assumed to follow a uniform distribution (i.e. that each value within the range is assumed equally likely to be the true one). Thus the standard deviation of each of these "input" variables can be easily calculated by using the formula $\frac{b-a}{\sqrt{12}}$, where a is the lower end point of the range and b the upper end point.

The values that will remain static throughout this examples set are as follows:

$$\mathbf{v}_0^T = \widetilde{\mathbf{v}}_0^T \left[\mathbf{M}(\boldsymbol{\theta}_0, \boldsymbol{\phi}_0)\right]^{-T} = (26.82, -0.70, -0.09);$$

$$\boldsymbol{\theta}_0^T = (\pi/6, 5\pi/6, 9\pi/6) = (0.5236, 2.6180, 4.7124).$$

Additionally, from the uniformity assumption and ranges discussed earlier, it can be deduced that

$$\sigma_{\widetilde{v}_j} = 0.0289,\ \sigma_{\theta_j} = \sigma_{\phi_j} = 5.7732 \times 10^{-4},\ j \in \mathcal{I}.$$

The examples below show the effect of varying the elevation angles of the LIDARs from low to high.

Demanded elevation angles, $\boldsymbol{\phi}_0^T$	$(\frac{\pi}{360}, \frac{\pi}{360}, \frac{\pi}{360})$**=(0.0087, 0.0087, 0.0087)**
Doppler velocity vector	**(22.8789, -23.5764, 0.6952)**
$\lvert\Delta(\boldsymbol{\theta}_0, \boldsymbol{\phi}_0)\rvert$	**0.0227**
Error formula std. devs, $s_{v_j}, j \in \mathcal{I}$, for uncertainty in recon. vel. components	**(0.0244, 0.0260, 2.0428)**
Comment: Noting that the elevation angles are just half a degree out from the horizontal plane, the measurement configuration is unable to accurately resolve the vertical wind velocity component, as evidenced by the vertical error standard deviation at 2.04 m/s.	

Demanded elevation angles, $\boldsymbol{\phi}_0^T$	$(\frac{\pi}{30}, \frac{\pi}{30}, \frac{\pi}{30})$**=(0.1047, 0.1047, 0.1047)**
Doppler velocity vector	**(22.7461, -23.4565, 0.6831)**
$\lvert\Delta(\boldsymbol{\theta}_0, \boldsymbol{\phi}_0)\rvert$	**0.2686**
Error formula std. devs, $s_{v_j}, j \in \mathcal{I}$, for uncertainty in recon. vel. components	**(0.0246, 0.0261, 0.1705)**

Demanded elevation angles, $\boldsymbol{\phi}_0^T$	$(\frac{\pi}{12}, \frac{\pi}{12}, \frac{\pi}{12})$**=(0.2618, 0.2618, 0.2618)**
Doppler velocity vector	**(22.0784, -22.7957, 0.6498)**
$\lvert\Delta(\boldsymbol{\theta}_0, \boldsymbol{\phi}_0)\rvert$	**0.6274**
Error formula std. devs, $s_{v_j}, j \in \mathcal{I}$, for uncertainty in recon. vel. components	**(0.0254, 0.0268, 0.0689)**

Demanded elevation angles, $\boldsymbol{\phi}_0^T$	$(\frac{\pi}{4}, \frac{\pi}{4}, \frac{\pi}{4})$**=(0.7854, 0.7854, 0.7854)**
Doppler velocity vector	**(16.1175, -16.7326, 0.4306)**
$\lvert\Delta(\boldsymbol{\theta}_0, \boldsymbol{\phi}_0)\rvert$	**0.9186**
Error formula std. devs, $s_{v_j}, j \in \mathcal{I}$, for uncertainty in recon. vel. components	**(0.0357, 0.0357, 0.0252)**

Demanded elevation angles, $\boldsymbol{\phi}_0^T$	$(\frac{5\pi}{12}, \frac{5\pi}{12}, \frac{5\pi}{12})$**=(1.3090, 1.3090, 1.3090)**
Doppler velocity vector	**(5.8379, -6.1861, 0.0961)**
$\lvert\Delta(\boldsymbol{\theta}_0, \boldsymbol{\phi}_0)\rvert$	**0.1681**
Error formula std. devs, $s_{v_j}, j \in \mathcal{I}$, for uncertainty in recon. vel. components	**(0.1000, 0.0947, 0.0185)**

Demanded elevation angles, $\boldsymbol{\phi}_0^T$	$(\frac{7\pi}{16}, \frac{7\pi}{16}, \frac{7\pi}{16})$=**(1.3744, 1.3744, 1.3744)**
Doppler velocity vector	**(4.3784 -4.6849 0.0505)**
$\lvert\Delta(\boldsymbol{\theta}_0, \boldsymbol{\phi}_0)\rvert$	**0.0970**
Error formula std. devs, $s_{v_j}, j \in \mathcal{I}$, for uncertainty in recon. vel. components	**(0.1329, 0.1254, 0.0182)**
Comment: Noting that the elevation angles are 78.75 degrees from the horizontal, all three beams are starting to approach being parallel along the vertical. Whilst the standard deviation for the vertical velocity error is reduced, those for the horizontal velocity errors have grown above the typical wind industry requirement of 0.1 m/s, as the horizontal velocity resolving power becomes reduced.	

As could have been anticipated, for low elevation angles, the first and second Cartesian velocity components will have standard deviations which are at the lower end of their ranges, whereas the third component will have a standard deviation at the higher end. At high elevation angles, one sees exactly the converse.

But interestingly, seemingly in line with the remarks of Section 3.3, we can clearly see a "$\frac{1}{\lvert\Delta(\boldsymbol{\theta}_0, \boldsymbol{\phi}_0)\rvert}$" phenomenon at play for low elevation angles in respect of the standard deviation of the third reconstructed vector component, namely s_{v_3}. This shows that in a practical field deployment of the converging beam triple LIDAR, it is advantageous to ensure that the measurement position is not close to the plane defined by the three LIDARs.

Examples Set 2

The settings will be exactly those as for Examples Set 1, except that

$$\boldsymbol{\phi}_0^T = (\pi/4, \pi/4, \pi/4) = (0.7854, 0.7854, 0.7854)$$

throughout, and

$$\boldsymbol{\theta}_0^T = (x, 5\pi/6, 9\pi/6) = (x, 2.6180, 4.7124);$$

where x will be varied such that $\pi/6 < x < 5\pi/6$, in order to show the effect of varying the azimuthal angle of the first LIDAR.

Demanded azimuthal angle of first LIDAR	$\frac{\pi}{4}$ **=0.7854**
Doppler velocity vector	**(13.0015, -16.7326, 0.4306)**
$\lvert\Delta(\boldsymbol{\theta}_0, \boldsymbol{\phi}_0)\rvert$	**0.8977**
Error formula std. devs, $s_{v_j}, j \in \mathcal{I}$, for uncertainty in recon. vel. components	**(0.0392, 0.0332, 0.0254)**

Demanded azimuthal angle of first LIDAR	$\frac{\pi}{3}$ **=1.0472**
Doppler velocity vector	**(8.9953, -16.7326, 0.4306)**
$\lvert\Delta(\boldsymbol{\theta}_0, \boldsymbol{\phi}_0)\rvert$	**0.8365**
Error formula std. devs, $s_{v_j}, j \in \mathcal{I}$, for uncertainty in recon. vel. components	**(0.0447, 0.0312, 0.0261)**

Demanded azimuthal angle of first LIDAR	$\frac{\pi}{2}$ **=1.571**
Doppler velocity vector	**(-0.5537, -16.7326, 0.4306)**
$\lvert\Delta(\boldsymbol{\theta}_0, \boldsymbol{\phi}_0)\rvert$	**0.6124**
Error formula std. devs, $s_{v_j}, j \in \mathcal{I}$, for uncertainty in recon. vel. components	**(0.0643, 0.0309, 0.0309)**

Demanded azimuthal angle of first LIDAR	$\frac{9\pi}{12}$ **=2.356**
Doppler velocity vector	**(-13.8205, -16.7326, 0.4306)**
$\lvert\Delta(\boldsymbol{\theta}_0, \boldsymbol{\phi}_0)\rvert$	**0.1477**
Error formula std. devs, $s_{v_j}, j \in \mathcal{I}$, for uncertainty in recon. vel. components	**(0.2384, 0.1180, 0.1199)**
Comment: Noting that with the azimuthal separation of two of the beams being reduced to just 15 degrees, then the standard deviations of the velocity reconstruction errors have grown beyond 0.1 m/s.	

Demanded azimuthal angle of first LIDAR	$\frac{19\pi}{24}$ **=2.487**
Doppler velocity vector	**(-15.4079, -16.7326, 0.4306)**
$\lvert\Delta(\boldsymbol{\theta}_0, \boldsymbol{\phi}_0)\rvert$	**0.0718**
Error formula std. devs, $s_{v_j}, j \in \mathcal{I}$, for uncertainty in recon. vel. components	**(0.4731, 0.2528, 0.2538)**

Demanded azimuthal angle of first LIDAR	$\frac{39\pi}{48}$ **=2.553**
Doppler velocity vector	**(-16.1046, -16.7326, 0.4306)**
$\lvert\Delta(\boldsymbol{\theta}_0, \boldsymbol{\phi}_0)\rvert$	**0.0353**
Error formula std. devs, $s_{v_j}, j \in \mathcal{I}$, for uncertainty in recon. vel. components	**(0.9440, 0.5245, 0.5250)**
Comment: Noting that with the azimuthal separation of two of the beams being reduced to just 3.75 degrees, then the standard deviations of the velocity reconstruction errors have grown beyond 0.5 m/s.	

Again we observe an approximate "$\frac{1}{|\Delta(\boldsymbol{\theta}_0, \boldsymbol{\phi}_0)|}$" phenomenon manifesting itself, but this time across all three standard deviations for the reconstruction error in the Cartesian velocity components, at the lower end of the range for the azimuthal discrepancy between the first and second LIDARs. This shows that in a practical field deployment, it is advantageous to ensure that the azimuthal angle separation between the three LIDAR beams is maximized. If any two of the beams approach being parallel then this tends to increase the uncertainty associated with the reconstructed velocity vector.

5 Conclusions

In this paper the error propagation formulae have been presented for the static convergent beam LIDAR which can be applied especially in the wind energy industry (and potentially also in aviation, construction and transportation). By way of examples it is demonstrated to the practitioner how the formulae may be applied in order to govern deployment of a convergent beam LIDAR. Deployment of the converging beam LIDAR can take place at a prospective wind farm in order to assess three-dimensional wind conditions during the planning process. Alternatively the converging beam LIDAR can be deployed at an operating wind farm in order to understand three-dimensional wind conditions incident at a specific operational turbine, especially where the turbine is suspected of underperformance due to complex flow.

It should be noted that the numeric examples given in the previous section are for the sake of illustration. In general, the results will depend also on the wind velocity being measured, which obviously varies in magnitude and relative orientation. The possible error distribution may be calculated before undertaking a converging beam LIDAR measurement campaign, in order to ensure that a proposed deployment configuration is suitable for a given range of geometries and wind velocities. Some general principles apply:
(a) the estimated variances of the components of the reconstructed wind velocities tend to increase when measurement positions approach the plane defined by the three LIDAR locations;
(b) the estimated variances of the components of the reconstructed wind velocities tend to increase when the angle subtended at the measurement position, by any two LIDAR locations, becomes small.

Acknowledgements

`Wind Farm Analytics Ltd` would like to acknowledge the input and advice from the following people and organzations:
Dr Matthew Warden of `Fraunhofer UK Research Ltd` whose questions and discussion have prompted this work; Dr Henry Bookey, Dr Simon Sørensen and Dr John Macarthur from `Fraunhofer UK Research Ltd`; Dr Mark Silver, Dr Chris Watts and Engineer Ross Henderson of `Thales UK Ltd`;

`Wind Farm Analytics Ltd` would also like to thank `InnovateUK` for 70% funding the beginning of this work.

References

Billingsley, P. (1995), *Probability and Measure*, Third edn, Wiley.

Chatfield, C. & Collins, A. J. (1980), *Introduction to Multivariate Analysis*, Chapman and Hall.

EU Commission (2017), 'Third Report on the State of the Energy Union', *Brussels, 23.11.2017 COM(2017) 688 final* .

Fleming, P. A., Scholbrock, A. K., Jehu, A., Davoust, S., Osler, E., Wright, A. D. & Clifton, A. (2014), 'Field-test results using a nacelle-mounted lidar for improving wind turbine power capture by reducing yaw misalignment', *J. Phys.: Conf. Ser.* **524**.

Kreyszig, E. (1989), *Introductory Functional Analysis with Applications*, Revised edn, John Wiley & Sons.

Liu, J., Liu, H., Jiang, C., Han, X., Zhang, D. Q. & Hu, Y. I. (2018), 'A new measurement for structural uncertainty propagation based on pseudo-probability distribution', *Applied Mathematical Modelling* **63**.

Luenberger, D. G. (2005), *Introduction to Linear and Nonlinear Programming*, Second edn, Springer.

Mann, J., Cariou, J.-P., Courtney, M. S., Parmentier, R., Mikkelsen, T., Wagner, R., Lindelöw, P., Sjöholm, M. & Enevoldsen, K. (2008), 'Comparison of 3D turbulence measurements using three staring wind lidars and a sonic anemometer', *IOP Conf. Ser.: Earth Environ. Sci.* **1**.

MEASNET (2016), 'Evaluation of Site-Specific Wind Conditions'. Version 2, April 2016.

Ni, B. Y., Jiang, C. & Han, X. (2016), 'An improved multidimensional parallelepipe d non-probabilistic model for structural uncertainty analysis', *Applied Mathematical Modelling* **40**.

Peña et. al. (2015), Remote Sensing for Wind Energy, Technical report, Technical University of Denmark.

Sathe, A., Banta, R., Pauscher, L., Vogstad, K., Schlipf, D. & Wylie, S. (2015), Estimating Turbulence Statistics and Parameters from Ground- and Nacelle-Based Lidar Measurements: IEA Wind Expert Report, Technical report, Technical University of Denmark.

Taylor, J. R. (1997), *Introduction To Error Analysis: The Study of Uncertainties in Physical Measurements*, Second edn, University Science Books.

UK Department of Business, Energy and Industrial Strategy (2018), 'Clean Growth Strategy - Leading the way to a low carbon future'.

UK Department of Energy and Climate Change (2013), 'UK Renewable Energy Roadmap: 2013 Update'.

Wagner, R., Courtney, M., Gottschall, J. & Lindelöw-Marsden, P. (2011), 'Accounting for the speed shear in wind turbine power performance measurement', *Wind Energy* **14**.

Wang, L., Xiong, C., Wang, X., Xu, M. & Li, Y. (2018), 'A dimension-wise method and its improvement for multidisciplinary interval uncertainty analysis', *Applied Mathematical Modelling* **59**.

Appendix

Detailed Proof of Theorem 1

We will work with the inner product space on $\mathbb{R}^9$, where, for $\mathbf{y}, \mathbf{z} \in \mathbb{R}^9$, the inner product $< \cdot, \cdot >$ is given by

$$< \mathbf{y}, \mathbf{z} >= \mathbf{y}^T \mathbf{z}$$

with induced Euclidian norm, $|| \cdot ||$, given by

$$||\mathbf{y}|| = \sqrt{\mathbf{y}^T \mathbf{y}}.$$

Working with the triangle inequality

$$|\text{Err}((\boldsymbol{\theta}_0, \boldsymbol{\phi}_0, \widetilde{\mathbf{v}}_0), (\boldsymbol{\theta}^*, \boldsymbol{\phi}^*, \widetilde{\mathbf{v}}^*))|$$

$$\leq \frac{1}{4}|\text{var}\left(\boldsymbol{\delta x}(\boldsymbol{\theta}_0, \boldsymbol{\phi}_0, \widetilde{\mathbf{v}}_0)^T \mathcal{H}_j(\gamma(\boldsymbol{\theta}_0, \boldsymbol{\phi}_0, \widetilde{\mathbf{v}}_0) + (1-\gamma)(\boldsymbol{\theta}^*, \boldsymbol{\phi}^*, \widetilde{\mathbf{v}}^*))\boldsymbol{\delta x}(\boldsymbol{\theta}_0, \boldsymbol{\phi}_0, \widetilde{\mathbf{v}}_0)\right)|$$

$$+|\text{cov}\left(\mathbf{g}_j^T(\boldsymbol{\theta}_0, \boldsymbol{\phi}_0, \widetilde{\mathbf{v}}_0)\boldsymbol{\delta x}(\boldsymbol{\theta}_0, \boldsymbol{\phi}_0, \widetilde{\mathbf{v}}_0), \boldsymbol{\delta x}(\boldsymbol{\theta}_0, \boldsymbol{\phi}_0, \widetilde{\mathbf{v}}_0)^T \mathcal{H}_j(\gamma(\boldsymbol{\theta}_0, \boldsymbol{\phi}_0, \widetilde{\mathbf{v}}_0) + (1-\gamma)(\boldsymbol{\theta}^*, \boldsymbol{\phi}^*, \widetilde{\mathbf{v}}^*))\boldsymbol{\delta x}(\boldsymbol{\theta}_0, \boldsymbol{\phi}_0, \widetilde{\mathbf{v}}_0)\right)|$$

$$\leq \frac{1}{4}\left|E\left[\left\{\boldsymbol{\delta x}(\boldsymbol{\theta}_0, \boldsymbol{\phi}_0, \widetilde{\mathbf{v}}_0)^T \mathcal{H}_j(\gamma(\boldsymbol{\theta}_0, \boldsymbol{\phi}_0, \widetilde{\mathbf{v}}_0) + (1-\gamma)(\boldsymbol{\theta}^*, \boldsymbol{\phi}^*, \widetilde{\mathbf{v}}^*))\boldsymbol{\delta x}(\boldsymbol{\theta}_0, \boldsymbol{\phi}_0, \widetilde{\mathbf{v}}_0)\right\}^2\right]\right|$$

$$+\frac{1}{4}\left|E\left[\boldsymbol{\delta x}(\boldsymbol{\theta}_0, \boldsymbol{\phi}_0, \widetilde{\mathbf{v}}_0)^T \mathcal{H}_j(\gamma(\boldsymbol{\theta}_0, \boldsymbol{\phi}_0, \widetilde{\mathbf{v}}_0) + (1-\gamma)(\boldsymbol{\theta}^*, \boldsymbol{\phi}^*, \widetilde{\mathbf{v}}^*))\boldsymbol{\delta x}(\boldsymbol{\theta}_0, \boldsymbol{\phi}_0, \widetilde{\mathbf{v}}_0)\right]\right|^2$$

$$+\left|E\left[\left\{\mathbf{g}_j^T(\boldsymbol{\theta}_0,\boldsymbol{\phi}_0,\widetilde{\mathbf{v}}_0)\boldsymbol{\delta x}(\boldsymbol{\theta}_0,\boldsymbol{\phi}_0,\widetilde{\mathbf{v}}_0)\right\}\left\{\boldsymbol{\delta x}(\boldsymbol{\theta}_0,\boldsymbol{\phi}_0,\widetilde{\mathbf{v}}_0)^T\mathcal{H}_j(\gamma(\boldsymbol{\theta}_0,\boldsymbol{\phi}_0,\widetilde{\mathbf{v}}_0)+(1-\gamma)(\boldsymbol{\theta}^*,\boldsymbol{\phi}^*,\widetilde{\mathbf{v}}^*))\boldsymbol{\delta x}(\boldsymbol{\theta}_0,\boldsymbol{\phi}_0,\widetilde{\mathbf{v}}_0)\right\}\right]\right|$$
$$+\left|E\left[\mathbf{g}_j^T(\boldsymbol{\theta}_0,\boldsymbol{\phi}_0,\widetilde{\mathbf{v}}_0)\boldsymbol{\delta x}(\boldsymbol{\theta}_0,\boldsymbol{\phi}_0,\widetilde{\mathbf{v}}_0)\right]\right|\times\left|E\left[\boldsymbol{\delta x}(\boldsymbol{\theta}_0,\boldsymbol{\phi}_0,\widetilde{\mathbf{v}}_0)^T\mathcal{H}_j(\gamma(\boldsymbol{\theta}_0,\boldsymbol{\phi}_0,\widetilde{\mathbf{v}}_0)+(1-\gamma)(\boldsymbol{\theta}^*,\boldsymbol{\phi}^*,\widetilde{\mathbf{v}}^*))\boldsymbol{\delta x}(\boldsymbol{\theta}_0,\boldsymbol{\phi}_0,\widetilde{\mathbf{v}}_0)\right]\right|. \tag{29}$$

Since $\mathcal{H}_j(\gamma(\boldsymbol{\theta}_0,\boldsymbol{\phi}_0,\widetilde{\mathbf{v}}_0)+(1-\gamma)(\boldsymbol{\theta}^*,\boldsymbol{\phi}^*,\widetilde{\mathbf{v}}^*)):\mathbb{R}^9\mapsto\mathbb{R}^9$ is a bounded linear operator, then we can induce its norm in the standard way (see Kreyszig (1989) for example).
Through a combination of:
• using Jensen's inequality (see Billingsley (1995) for example), for taking the absolute value norm, $|\cdot|$ (which is convex on $\mathbb{R}$), inside the expectation operators;
• moving from the absolute value norm, $|\cdot|$, through to a bound in terms of the Euclidean norm, defined on $\mathbb{R}^9$, via use of the Cauchy-Schwarz inequality;
• using the *compatibility* property, that is automatically satisfied by induced matrix norms;
then we can bound (29) by

$$\frac{1}{4}\left(E[||\boldsymbol{\delta x}(\boldsymbol{\theta}_0,\boldsymbol{\phi}_0,\widetilde{\mathbf{v}}_0)||^4||\mathcal{H}_j(\gamma(\boldsymbol{\theta}_0,\boldsymbol{\phi}_0,\widetilde{\mathbf{v}}_0)+(1-\gamma)(\boldsymbol{\theta}^*,\boldsymbol{\phi}^*,\widetilde{\mathbf{v}}^*))||^2]\right.$$
$$\left.+\frac{1}{4}E[||\boldsymbol{\delta x}(\boldsymbol{\theta}_0,\boldsymbol{\phi}_0,\widetilde{\mathbf{v}}_0)||^2||\mathcal{H}_j(\gamma(\boldsymbol{\theta}_0,\boldsymbol{\phi}_0,\widetilde{\mathbf{v}}_0)+(1-\gamma)(\boldsymbol{\theta}^*,\boldsymbol{\phi}^*,\widetilde{\mathbf{v}}^*))||]^2\right)$$
$$+E[||\boldsymbol{\delta x}(\boldsymbol{\theta}_0,\boldsymbol{\phi}_0,\widetilde{\mathbf{v}}_0)||^3||\mathbf{g}_j(\boldsymbol{\theta}_0,\boldsymbol{\phi}_0,\widetilde{\mathbf{v}}_0)||||\mathcal{H}_j(\gamma(\boldsymbol{\theta}_0,\boldsymbol{\phi}_0,\widetilde{\mathbf{v}}_0)+(1-\gamma)(\boldsymbol{\theta}^*,\boldsymbol{\phi}^*,\widetilde{\mathbf{v}}^*))||]$$
$$+E[||\boldsymbol{\delta x}(\boldsymbol{\theta}_0,\boldsymbol{\phi}_0,\widetilde{\mathbf{v}}_0)||||\mathbf{g}_j(\boldsymbol{\theta}_0,\boldsymbol{\phi}_0,\widetilde{\mathbf{v}}_0)||]E[||\boldsymbol{\delta x}(\boldsymbol{\theta}_0,\boldsymbol{\phi}_0,\widetilde{\mathbf{v}}_0)||^2||\mathcal{H}_j(\gamma(\boldsymbol{\theta}_0,\boldsymbol{\phi}_0,\widetilde{\mathbf{v}}_0)+(1-\gamma)(\boldsymbol{\theta}^*,\boldsymbol{\phi}^*,\widetilde{\mathbf{v}}^*))||]. \tag{30}$$

Clearly $v_j(\cdot,\cdot,\cdot)$ is twice continuously differentiable over a compact set $\mathcal{X}$, in the sense that all of its first and second partial derivatives (mixed, or otherwise) are continuous over such a set. It can be deduced, therefore, that $||\mathcal{H}_j(\cdot)||$ is continuous with respect to γ (which can be seen to be a consequence of the fact that, for two matrices $X,Y:\mathbb{R}^9\mapsto\mathbb{R}^9$, say: (i) from the triangle inequality $\big|||X||-||Y||\big|\leq||X-Y||$; and (ii) the induced norm matrix is *equivalent* to any *entrywise* matrix norm). Hence there exists a finite scalar, $\mathcal{H}_j^{\max}(\boldsymbol{\theta}_0,\boldsymbol{\phi}_0,\widetilde{\mathbf{v}}_0)$, such that

$$||\mathcal{H}_j(\gamma(\boldsymbol{\theta}_0,\boldsymbol{\phi}_0,\widetilde{\mathbf{v}}_0)+(1-\gamma)(\boldsymbol{\theta}^*,\boldsymbol{\phi}^*,\widetilde{\mathbf{v}}^*))||\leq\mathcal{H}_j^{\max}(\boldsymbol{\theta}_0,\boldsymbol{\phi}_0,\widetilde{\mathbf{v}}_0)$$

for all $0\leq\gamma\leq1$. Indeed, one might select $\mathcal{H}_j^{\max}(\boldsymbol{\theta}_0,\boldsymbol{\phi}_0,\widetilde{\mathbf{v}}_0)$ to serve as a bound over some appropriate superset of $\mathcal{X}$ in order to circumvent any dependence on a particular $(\boldsymbol{\theta}_0,\boldsymbol{\phi}_0,\widetilde{\mathbf{v}}_0)$. Also note that since $\boldsymbol{\delta x}(\boldsymbol{\theta}_0,\boldsymbol{\phi}_0,\widetilde{\mathbf{v}}_0)\in[-\mathcal{B},\mathcal{B}]^9$, then $||\boldsymbol{\delta x}(\boldsymbol{\theta}_0,\boldsymbol{\phi}_0,\widetilde{\mathbf{v}}_0)||\leq3\mathcal{B}$. Thus a further bound on (30) is given by

$$\frac{81}{2}\mathcal{B}^4(\mathcal{H}_j^{\max}(\boldsymbol{\theta}_0,\boldsymbol{\phi}_0,\widetilde{\mathbf{v}}_0))^2+54\mathcal{B}^3||\mathbf{g}_j(\boldsymbol{\theta}_0,\boldsymbol{\phi}_0,\widetilde{\mathbf{v}}_0)||\mathcal{H}_j^{\max}(\boldsymbol{\theta}_0,\boldsymbol{\phi}_0,\widetilde{\mathbf{v}}_0). \tag{31}$$

□